IEEE Access
Multidisciplinary ⋮ Rapid Review ⋮ Open Access Journal

Received 3 April 2022, accepted 20 April 2022, date of publication 22 April 2022,
date of current version 28 April 2022.

Digital Object Identifier 10.1109/ACCESS.2022.3169766

Analytic Solutions for Wheeled Mobile Manipulator Supporting Forces

GORAN R. PETROVIĆ AND JOUNI MATTILA
Faculty of Engineering and Natural Sciences, Unit of Automation Technology and Mechanical Engineering, Tampere University, 33100 Tampere, Finland
Corresponding author: Goran R. Petrović (goran.petrovic@tuni.fi)

This work was supported in part by the Shift2Rail Joint Undertaking (JU) under Agreement 101015418, and in part by the European Union's Horizon 2020 Research and Innovation Programme.

ABSTRACT When a mobile manipulator's wheel loses contact with the ground, the manipulator may overturn, causing material damage, and in the worst case, putting human lives in danger. The overturning stability of wheeled mobile manipulators must not be overlooked at any stage of the mobile manipulator's life, starting from the design phase, continuing through the commissioning period and extending to the operational phase. The various overturning stability criteria formulated throughout the years do not explicitly consider normal wheel loads, with most of them relying on the prescribed stability margins in terms of overturning moments. These formulations commonly consider the overturning moments regarding axes connecting the adjacent manipulator's contact points with the ground and could be notably restrictive. Explicit expressions for the supporting forces of the manipulator provide the best insights into the relevant affecting terms that contribute to the overturning (in)stability. They also reduce the necessity for considering about which axis the manipulator could overturn and simultaneously enable the formulation of more intuitive stability margins and on-line overturning prevention techniques. The present study presents a general dynamics modelling approach in the Newton–Euler framework using 6D vectors and provides normal wheel load equations for a typical 4-wheeled rigid-chassis mobile manipulator traversing uneven terrain. The given expressions are expected to become the standard guidelines in considered wheeled mobile manipulators and to provide a basis for effective overturning stability criteria and overturning avoidance techniques. Based on the presented results, specific improvements of the state-of-the-art criteria are discussed.

INDEX TERMS Mobile manipulators, multibody dynamics, tip-over monitoring, wheel normal loads.

I. INTRODUCTION

Mobile manipulators have considerable application potential in various fields such as mining, logging, construction, earth-moving, searching and rescuing, agriculture, and planetary exploration [1]–[3]. The overturning stability of these vehicles equipped with a manipulator arm is crucial regardless of the level of automation. Heavy-duty mobile manipulators face the risk of overturning if operated inadequately by an unskilled (tele)operator and in case of unexpected occurrences. Slope negotiations in sites where soil may also be unstable can be incredibly challenging [4]. In dexterous, manoeuvrable, compact, and lightweight robots, the risk of overturning is due to a high centre of mass (COM) and small weight and ground base, especially in combination with high loads and accelerations [5].

Simple thought experiments can suffice to introduce the motivation for the following analysis. Let us consider, for example, a lightweight wheeled platform that carries a manipulator arm of comparable weight. It is intuitively clear that overturning can occur under specific disadvantageous arm postures, especially with external forces acting on the manipulator tip, for example, when carrying a load or interacting with surroundings. An additional aggravating factor, in this case, can be sloped and rugged terrain. Overturning begins by making one or more ground reactions equal to zero at first; then, if some preventive action is not taken in time, material and collateral damage are imminent. Although the mobile manipulator will eventually topple on one of its sides, loss of contact with the ground for one wheel is a reason for alarm. Extra special care must be taken

The associate editor coordinating the review of this manuscript and approving it for publication was Hassen Ouakad.

if a manipulator–human interaction is occurring. In other *mise-en-scène*, where a human-operated heavy-duty mobile manipulator (e.g., an excavator) is working in an environment with other people nearby, human lives can be at stake in a severe turn of events if overturning occurs. These considerations in two different settings also emphasise the significance of monitoring tyre loads even in semi- and non-automated solutions, making overturning stability indicators necessary in regular everyday use. However, in the absence of (tele)operator action, fully automated solutions rely wholly on how well the overturning stability indicator is formulated.

The overturning analysis of a mobile manipulator should come into focus starting from the early design stages where the number of wheels, size, mass, the position of the manipulator arm and, possibly, other manipulator parameters are optimised to maximise the workspace and provide the relative stability margin against overturning in the most critical predicted cases [6]. Even detailed analyses such as these, performed in advance, may not be able to anticipate the specific, unexpected course of events during operation. Thus, overturning monitoring should create an alert and start the overturning avoidance sequence whenever an overturning danger exists.

A well-defined overturning stability indicator may explicitly or implicitly address the wheel supporting forces. It must also include all the relevant factors that affect the forces. Although the relevance of each one, *per se*, might not be the same from case to case, all potentially influential factors must be preliminarily considered in a general contemplation. These include all the system masses and moments of inertia, together with all the significant linear/angular accelerations/velocities/positions and terrain slopes.

As the literature review in Section II shows, overturning stability monitoring in wheeled mobile manipulators has received significant attention continuously over the years. Although various approaches with different underlying concepts and modelling complexities have been proposed, the methods usually lack detailed expressions for normal loads and overturning stability criteria considering the supporting forces accompanied by full-dynamics modelling. It must be noted that for some reason, a gap exists between the fields of research of car and mobile manipulators in calculating wheel supporting forces, although weight transfer to tyres is a common sphere of interest. Once this particular gap is overcome and the expanded expressions for normal tyre loads are derived from the full-dynamics model, overturning axes will not have to be considered any more.

The overturning criterion can be formulated most naturally in terms of normal loads. By monitoring normal wheel loads, one can effectively trace if the value of any supporting forces approaches some prescribed critical value, which is an intuitive problem solution.

As the main contribution, the present study closes one existing gap between car and mobile manipulator dynamics by providing an extension of expressions for normal car wheel loads to the case where a manipulator arm exists on top of a wheeled platform. We further show how the overturning stability indicator based on wheel loads removes the need for addressing overturning axes, while neither imposing additional restrictions nor being computationally demanding. Appropriate alternatives to the state-of-the-art overturning criteria are suggested but do not take the central focus here.

The present study provides a detailed dynamics model, under the veil of the Newton–Euler (N–E) formalism using 6D vectors of a 4-all-wheel-drive (4AWD) rigid-chassis mobile manipulator negotiating uneven terrain. The specimen 4AWD mobile manipulator is chosen for analysis since it offers a fair amount of generality without introducing excessive complexity. Heavy-duty machines with Ackermann or skid steering can be considered special cases of the case presented here. Additional efforts must be made in the case of articulated steering and in the case of six or more wheels. The special wheel-legged chassis case in which the position of the wheels can be adjusted during operation must be also analysed separately and is not covered by the present study. Because the same reasoning and line of thought as presented here should be followed in those situations, they will not receive special attention in the following analysis.

Subsystem-by-subsystem modelling and underlying analysis were performed in detail with a minimum number of reasonable assumptions to balance the complexity and practicality with the modelling accuracy. Expressions for normal wheel loads are derived in a neat and structured manner. These provide the basis for the proposed overturning force (OTF) criterion, which does not rely on a typically used overturning axis, and can be considered as a quick and better alternative to the state-of-the-art criteria. It is expected that this or similar criteria will become a de-facto standard overturning stability indicator in mobile manipulators. Having explicit expressions for normal wheel loads makes it easy to perform term-by-term analysis starting from the design phase. It also makes the formulation of overturning prevention actions more straightforward. Apart from getting good general insights, end-users will also be able to tailor the given expressions according to their own needs.

The validity of the derived expressions for normal forces is verified in the Simscape Multibody^{TM} by comparing results to the unbiased reference from the renowned software.

The rest of the paper is organised as follows. Section II gives a literature overview to situate the present study better. Section III motivates the use of the N–E formalism in the discussed context. Section IV presents the essential mathematical preliminaries. Section V addresses the kinematics of a mobile manipulator negotiating a slope. Section VI provides 6D vector models of the wheel and chassis dynamics. Section VII deals with equations whose solutions are tyre-supporting forces. Section VIII presents the simulation results and suggests improvements of relevant tip-over stability and avoidance criteria along with parameter uncertainty analysis. Section IX contemplates the obtained results. Section X summarises the conclusions drawn.

II. LITERATURE REVIEW

The idea of the zero moment point (ZMP), [7], addresses a point on the ground where the resultant moment of the external and inertial forces is equal to zero. Initially proposed in [8] for use in mobile manipulators, referring to the position of the ZMP with respect to the stability polygon, it has remained a key aspect of the research on overturning stability and related topics. Often, remarkably simplified dynamics models are combined with ZMP, and this fact has been a common cause for criticism in the mobile-manipulator community. Using the ZMP-based stability criterion from paper [9], paper [10] reported that the ZMP is a less sensitive indicator than the Force-Angle (FA) or Moment-Height Stability (MHS) for certain mobile manipulators. However, ZMP has proven to be helpful in on-line trajectory planning both for light and heavy mobile manipulators [11]–[13] and for quadrupedal ones with wheels [14]. It contrasts the full-dynamics modelling narrative promoted here, with the primary aim being deriving expressions for supporting forces.

Continuing efforts on developing improved tip-over indicators gave rise to the FA indicator [15], with heavy-duty mobile machines serving as the primary source of inspiration. Note that this criterion would provide a relevant and reliable indication at low speeds and with external forces of large magnitudes. The FA stability indicator considers the angle between the net force (excluding the ground support reaction forces) reduced to the planar mass system's COM and the rays connecting the same COM with the ground connection points. A vital aspect of the discussion concerns the tipping-over axis. *Natural tip-over* and *tripped tip-over* notions have been introduced. The tip-over is considered natural if overturning occurs about one of the axes connecting the manipulator support points in contact with the ground (support polygon vertices). The tripped tip-over occurs about an axis representing a linear combination of the abovementioned axes. Examination of the tripped tip-over seems to be abandoned in mainstream research, and it will be recalled here. A FA tip-over prevention algorithm was presented in [16].

In [17], also assuming that tipping-over will occur about one of the axes connecting the manipulator wheels, the MHS stability criterion was formulated utilising the overturning moments without explicitly addressing ground reactions. A simple method to include the chassis COM height was presented and created a significant impact. Being a direct consequence of the dynamics modelling in the N–E framework, it has neatly brought focus to forces/moments acting at the chassis/manipulator base connection. The formulation has opened a path to more detailed stability criteria by explicitly addressing certain key factors in the normal load analysis. An on-line tip-over prevention MHS-based criterion was proposed in [18] and was compared to the FA-method based.

The study [19] resumed the established trend of formulating tipping-over stability indicators using moments about the manipulator supporting polygon axes. The Tipping Over Moment (TOM) criterion is an extended and improved version of the MHS. It includes the wheeled platform weight in the analysis and presents a reasonably formulated criterion, which, similarly to its predecessor MHS, does not explicitly consider the inertial forces and ground reactions of the wheeled platform. The TOM essentially investigates the values of the anti-tipping-over moment, referring to the negative moment values as the ones providing stability. These moments are compared to the prescribed relative stability margin values, as in paper [20] for a dual-armed wheel robot. In [21], the TOM was used to calculate the deceleration of a mobile manipulator such that tip-over was prevented.

By examining the research trends in the tip-over stability of mobile manipulators, researchers have attempted to improve the TOM by performing modelling with fewer approximations in a usable manner. In the study [22], a significant Improved Tipping Over Moment (ITOM) indicator was proposed. This indicator is qualified to be named like that because it includes a wheeled platform's inertial forces in the TOM. These forces have been usually neglected terms throughout the years in this line of research, although they are undoubtedly worth considering, in light of the significant dynamic coupling between the manipulator arm and the wheeled platform. The analysis which led to the ITOM formulation considered a manipulator negotiating a constant slope in the direction of motion. As with TOM, tipping-over axes with ITOM were again assumed to connect vertices of the support polygon, and thus, the supporting forces were not explicitly considered. It was also argued that analytic expressions for ITOM are hard to obtain. A complex manipulator arm inevitably leads to complicated equations of motion; however, with careful rearrangement in a structured manner, many significant insights can be obtained from neat analytic expressions. Although specific challenges exist, it is plausible to obtain relatively simple analytic expressions for supporting forces by expanding ideas from car dynamics.

A detailed discussion regarding the terrain slope has usually been avoided when the tip-over stability was examined. Commonly, two Euler angles at most were considered to be sufficient to describe the orientation of the chassis to the inertial frame of reference, fixed in the earth-tangent plane. Interestingly enough, weight transfer to wheels of an accelerating platform negotiating a slope has been an omnipresent topic in car dynamics, [23].

Weight transfer to the wheels, i.e. the tyre normal load, had always required special attention in the field of car dynamics because the standard tyre/road interaction models use the normal force to calculate the remaining tyre/road forces/moments, [24]–[25]. Thus, this issue has been recognised and has been widely addressed, usually providing approximate expressions which are sufficient to address car motion. The problem of quantifying wheel loads becomes complicated in mobile manipulators with a manipulator arm attached to the chassis and interacting with the surroundings. In the general case, where the tyre weight can not be neglected, and both manipulator posture and movements will

affect the normal tyre load, existing straightforward expressions require an extension.

An effort for explicitly formulating a tipping-over stability criterion using wheel loads can be found in [26], in which the analysis of the dynamics is over-simplified. Explicit formulation using normal wheel loads is experimentally addressed in [27] on a small-scale laboratory test bench. However, because the discussed approach requires the measurement of normal loads, it falls out of the perspective for the proposed narrative because of the high cost and potentially impossible force sensor integrity preservation in heavy-duty mobile manipulators. Explicit formulation of the stability criterion in terms of the wheel loads for a 3-wheeled mobile robot together with real-time tip-over prevention and path following control using fuzzy and neural-fuzzy approaches can be found in [28]. Related detailed derivations, in this 3-wheeled case, have been provided in the predecessor paper [29], which also advocates the monitoring of normal wheel forces.

A recent study assessing the rollover risk in a 4-wheeled articulated-steering vehicle recognized the case in which one wheel off the ground is the dangerous state [30]. The authors used neural networks to estimate the rollover risk probability without detailed dynamics modelling, exploiting experimental data.

References [31]–[32] provide detailed models for articulated-steering and wheel-legged manipulators, respectively. These models are extensive and were verified using renowned software; however, they both provide expressions for normal forces as proportional to tyre and spring deformation, respectively. This way to model the wheel loads in simulation software is one of the best and most common [3], [33], and these expressions are known to provide reliable numerical solutions. Written like this, they deal with consequences rather than causes and induce the need for likely retroactive decision-making regarding the relevant factors in overturning stability. *The present study intends to raise awareness of the need to reformulate expressions for normal wheel forces in all relevant steering configurations, following the presented ideas.*

Based on the literature review above, the present study aims to provide a solution for the identified gap between car and mobile manipulator dynamics. By removing the overturning axis restrictions, we aim to establish a trend of monitoring supporting forces as the most relevant overturning stability factor in wheeled mobile manipulators.

III. CHOOSING THE MODELLING FORMALISM

Among the various approaches for dynamics modelling, the Lagrange formulation, which is based on kinetic and potential energies, and the N–E formulation, which is based on the balance of forces acting on a rigid manipulator link, are the most common, with the N–E approach considered as more fundamental [34].

In the recursive N–E algorithm (RNEA), the number of computations linearly increases with the number of degrees of freedom (DOF). Using the RNEA, linear/angular velocity vectors are calculated from a manipulator arm base to a manipulator arm tip. Forces/moments are calculated in the reverse order, going from the manipulator arm tip to the arm base. In the case of mobile manipulators, it will be interesting to note that the kinematics analysis starts with the chassis and branches towards each wheel and the manipulator arm tool centre-point (TCP). Irrespectively of the underlying case, kinematic relations must first be appropriately established because all the subsequent results depend on them.

Reformulations of the RNEA equations using 6D vectors where linear and angular velocities are stacked together, apart from leading to the more compact notation, allow a problem be solved more directly, at a higher level of abstraction, [35]. Mathematical models formulated using the 6D vector RNEA are also indispensable, for example, in the virtual decomposition control (VDC) field of research, [36].

Apart from the 6D RNEA benefits mentioned above, the primary motivation for using the N–E formulation here is that the free-body diagram analysis allows the direct inclusion of ground reaction forces in the dynamics analysis. In line with this direct inclusion of the manipulator supporting forces, all relevant geometric and inertial properties are naturally included in the expressions, which will be derived here as the main result.

A 6D vector dynamics model of a mobile manipulator will be derived starting with the derivation of a wheel dynamics model, followed by that of a chassis dynamics model. As a manipulator arm, a serial-parallel hydraulic manipulator will be used and modelled using the state-of-the-art N–E model given in [37], although any N–E model of any manipulator arm would fit in the proposed narrative.

IV. MATHEMATICAL PRELIMINARIES

Inevitable terms and notions are presented here from [38].

Every rigid body in the analysis will have at least one three-dimensional coordinate system $\{A\}$ (called frame $\{A\}$ in the following text) attached to it.

Let the linear and angular velocities as sensed in frame $\{A\}$ be denoted throughout the paper as ${}^A\boldsymbol{v} = \left({}^Av_x\ {}^Av_y\ {}^Av_z\right)^T$ and ${}^A\boldsymbol{\omega} = \left({}^A\omega_x\ {}^A\omega_y\ {}^A\omega_z\right)^T$, respectively. Furthermore, adopting the notation from [38], the 6D linear/angular velocity vector in frame $\{A\}$ is given as follows:

$$ {}^A\boldsymbol{V} = \begin{pmatrix} {}^A\boldsymbol{v}^T & {}^A\boldsymbol{\omega}^T \end{pmatrix}^T \in \mathbb{R}^6. \tag{1} $$

Let the force and moment vectors applied to the origin of frame $\{A\}$ be similarly denoted as velocities using notation ${}^A\boldsymbol{f} = \left({}^Af_x\ {}^Af_y\ {}^Af_z\right)^T$ for forces and similar notation ${}^A\boldsymbol{m} = \left({}^Am_x\ {}^Am_y\ {}^Am_z\right)^T$ for moments. Similar to (1), the 6D force/moment vector, as sensed and expressed in frame $\{A\}$, is introduced as follows:

$$ {}^A\boldsymbol{F} = \begin{pmatrix} {}^A\boldsymbol{f}^T & {}^A\boldsymbol{m}^T \end{pmatrix}^T \in \mathbb{R}^6. \tag{2} $$

Furthermore, let frame $\{B\}$ be attached to the same rigid body as frame $\{A\}$. Moving the force from the origin of frame $\{A\}$ to the origin of frame $\{B\}$ introduces the moment of that

force about the origin of frame $\{B\}$. Then, quantities from (1) and (2) can be transformed among the frames using relations:

$$^{B}\boldsymbol{V} = {}^{A}\mathbf{U}_{\mathbf{B}}^{T}\,{}^{A}\boldsymbol{V}, \tag{3}$$

and

$$^{A}\boldsymbol{F} = {}^{A}\mathbf{U}_{\mathbf{B}}\,{}^{B}\boldsymbol{F}, \tag{4}$$

where ${}^{A}\mathbf{U}_{\mathbf{B}} \in \mathbb{R}^{6\times6}$ in (3) and (4) is a force/moment transformation matrix, transforming the force/moment vector measured and expressed in frame $\{B\}$ to the same force/moment vector measured and expressed in frame $\{A\}$. The transformation matrix can be further written as follows:

$${}^{A}\mathbf{U}_{\mathbf{B}} = \begin{pmatrix} {}^{A}\mathbf{R}_{\mathbf{B}} & \mathbf{O}_{3\times3} \\ \left({}^{A}\boldsymbol{r}_{\mathbf{AB}}\times\right){}^{A}\mathbf{R}_{\mathbf{B}} & {}^{A}\mathbf{R}_{\mathbf{B}} \end{pmatrix}, \tag{5}$$

where ${}^{A}\mathbf{R}_{\mathbf{B}} \in \mathbb{R}^{3\times3}$ is a rotation (direction cosine) matrix from frame $\{A\}$ to frame $\{B\}$, $\mathbf{O}_{3\times3}$ denotes a 3-by-3 zero-matrix, and $\left({}^{A}\boldsymbol{r}_{\mathbf{AB}}\times\right)$ in (5) is a skew-symmetric matrix operator, intended for cross-product calculation, which is defined as follows:

$$\left({}^{A}\boldsymbol{r}_{\mathbf{AB}}\times\right) = \begin{pmatrix} 0 & -r_z & r_y \\ r_z & 0 & -r_x \\ -r_y & r_x & 0 \end{pmatrix}, \tag{6}$$

with r_x, r_y and r_z denoting distances from the origin of frame $\{A\}$ to the origin of frame $\{B\}$ along the frame $\{A\}$ x-, y- and z-axis, respectively.

The net force/moment vector ${}^{A}\boldsymbol{F}^{*} \in \mathbb{R}^{6}$ of a rigid body in frame $\{A\}$ is defined as follows:

$$\mathbf{M}_{A}\frac{d}{\mathrm{d}t}\left({}^{A}\boldsymbol{V}\right) + \mathbf{C}_{A}\left({}^{A}\boldsymbol{\omega}\right){}^{A}\boldsymbol{V} + \mathbf{G}_{A} = {}^{A}\boldsymbol{F}^{*}, \tag{7}$$

where $\mathbf{M}_{A} \in \mathbb{R}^{6\times6}$ is the mass matrix, $\mathbf{C}_{A}\left({}^{A}\boldsymbol{\omega}\right) \in \mathbb{R}^{6\times6}$ is the matrix of Coriolis and centrifugal terms, and $\mathbf{G}_{A} \in \mathbb{R}^{6}$ includes the gravity terms. Detailed expressions for matrices in (7) when a body-fixed frame adopts all the body motions are given in [38]. In cases when it is not convenient for the underlying analysis to assume that the body-fixed frame adopts all the body motions, as will be here when analysing wheel dynamics, a straightforward application of expressions from [38] is not possible, and reformulation is required.

V. KINEMATIC CHAIN

Let us observe a rigid chassis of a mobile manipulator negotiating a slope in Fig. 1. Manipulator arm and wheels are not shown here for the sake of visibility and clarity. Their respective orientations are defined relative to the chassis orientation and will be addressed when required and appropriate.

For the sake of clarity, it is necessary to address certain underlying assumptions before proceeding with the analysis since they will strongly affect the derivation of kinematics and dynamics relations.

Assumption 1: "Flat-Earth" equations sufficiently describe the mobile manipulator dynamics.

Corollary 1 [39]: Description of the dynamic behaviour of a mobile manipulator over a small area of non-rotating Earth is sufficiently exact for the simulation and analysis needs.

Earth-fixed frame $\{\mathbf{G}\}$ $(OXYZ)$ from Fig. 1 will be considered as the inertial frame throughout the following analysis. The body-fixed frame $\{\mathbf{B_C}\}$ $(Cx_{\mathrm{BC}}y_{\mathrm{BC}}z_{\mathrm{BC}})$ with its origin in the chassis COM is chosen to adopt all the linear/angular body motions.

The transformation matrix relating frames $\{\mathbf{G}\}$ and $\{\mathbf{B_C}\}$ will be given by the $y_{\mathrm{BC}} - x_{\mathrm{BC}} - z_{\mathrm{BC}}$ rotation sequence to align the two considered frames. It is given with (8), as shown at the bottom of the page.

The angles Φ and Θ are related to the terrain slope, and angle Ψ is related to the orientation in the local ground plane, as illustrated in Fig. 1. A rotation matrix that relates the body $\{\mathbf{B_C}\}$ and inertial frame of reference $\{\mathbf{G}\}$ enables easy extraction of the angular velocity components in the $\{\mathbf{B_C}\}$ frame from the skew-symmetric matrix:

$$\left({}^{\mathbf{B_C}}_{\mathbf{G}}\boldsymbol{\omega}_{\mathbf{B_C}}\times\right) = {}^{\mathbf{B_C}}\mathbf{R}_{\mathbf{G}}\,{}^{\mathbf{G}}\dot{\mathbf{R}}_{B_C}, \tag{9}$$

which is formed per pattern in (6), and where ${}^{\mathbf{B_C}}_{\mathbf{G}}\boldsymbol{\omega}_{\mathbf{B_C}}$ labels the angular velocity of the chassis with respect to the inertial frame of reference $\{\mathbf{G}\}$, expressed in the $\{\mathbf{B_C}\}$ frame. The angular velocity is obtained by employing (8) in (9) in combination with (6), which provides the following:

$${}^{\mathbf{B_C}}_{\mathbf{G}}\boldsymbol{\omega}_{\mathbf{B_C}} = \begin{pmatrix} \dot{\Phi}\cos\Psi + \dot{\Theta}\cos\Phi\sin\Psi \\ -\dot{\Phi}\sin\Psi + \dot{\Theta}\cos\Phi\cos\Psi \\ \dot{\Psi} - \dot{\Theta}\sin\Phi \end{pmatrix}, \tag{10}$$

which is one of the essential factors that is required to be known in the following kinematics and dynamics analysis.

A simple example motivates the discussion regarding the terrain slope properties. When a wheeled platform is transiting an uneven terrain, strictly speaking, in the general case, each wheel is experiencing different ground slope values and gradients. This traversing introduces an error in the calculations if the local terrain slopes beneath each wheel are not obtained and are not accounted for correctly, as could be done using reconstruction from high-density laser scans [40].

Not accounting for the terrain properties in detail may not be a significant issue, especially in the case of gentler terrains that possess no ruggedness. Even when the terrain is not locally placid, the introduced error may not be effective for a long time. These considerations also give rise to the idea of modifying the tip-over stability criterion to further emphasise the terrain slope properties.

$${}^{\mathbf{G}}\mathbf{R}_{\mathbf{B_C}} = \begin{pmatrix} \cos\Theta\cos\Psi + \sin\Theta\sin\Phi\sin\Psi & \cos\Psi\sin\Theta\sin\Phi - \cos\Theta\sin\Psi & \cos\Phi\sin\Theta \\ \cos\Phi\sin\Psi & \cos\Phi\cos\Psi & -\sin\Phi \\ -\cos\Psi\sin\Theta + \cos\Theta\sin\Phi\sin\Psi & \cos\Theta\cos\Psi\sin\Phi + \sin\Theta\sin\Psi & \cos\Theta\cos\Phi \end{pmatrix} \tag{8}$$

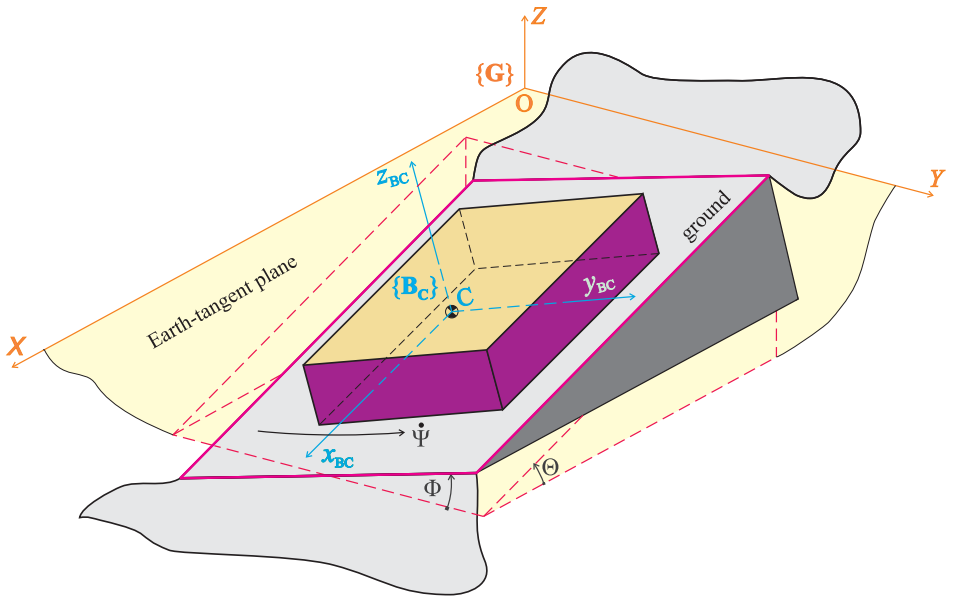

FIGURE 1. Knowing orientation of a manipulator chassis with respect to the Earth-tangent plane is essential when negotiating a slope.

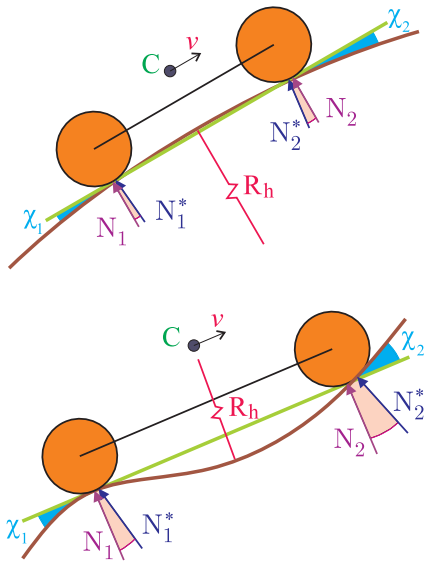

FIGURE 2. Effects of an uneven terrain.

Let us observe the planar situation from Fig. 2 that suffices to overlook the essential aspects of an uneven terrain motion and illustrate ideas related to the assumptions about to be introduced.

The effects of the traversing grade, crest, and dip have been well studied in the field of car dynamics and can be easily extended to the analysis here for the sake of completeness and generality, [41]–[42]. The centrifugal force affects wheel loading, and the differences in road curvature between the front and rear axle result in slightly different directions of normal axle forces. Normal forces with an asterisk subscript $N_i^*, i = 1, 2$ denote wheel forces acting in the exact direction, whereas N_i, $i = 1, 2$ denotes the normal forces acting in the approximately determined direction by knowing the chassis orientation with respect to the Earth-tangent plane. If the geometrical properties of the terrain are assumed to be unknown and are not accounted for, modelling errors are inevitable. Let us consider a set of commonly used assumptions for unknown terrain properties that are acceptable without introducing significant modelling errors. In addition, let us assume that a considered mobile manipulator will traverse an uneven terrain such that it decreases its velocity as the flatness of the terrain reduces. This situation is likely to be valid in practice and ensures that the centrifugal acceleration v^2/R_h does not have to be accounted for.

Assumption 2: The ratio of a manipulator COM velocity squared v^2 and the path curvature radius R_h is close to zero.

Corollary 2: The centrifugal acceleration is negligible and does not affect the wheel loads.

Not accounting for different directions of normal forces at the front and rear axle will introduce a certain modelling error that can not be avoided if these are not explicitly accounted for. Angles χ_1 and χ_2 from Fig. 2 illustrate these sources of the modelling errors. An efficient way to analyse this effect on the modelling error is to perform simulations in sophisticated software packages in which the terrain is given as a cloud of points. As the only possible and commonly used solution in these situations, where these angles are unknown, the following assumption on the terrain is introduced:

Assumption 3: All the wheels make contact with the same, locally flat, ground plane.

Corollary 3: The supporting forces acting on the manipulator wheels are mutually parallel.

Note that angle values Φ and Θ are dominant and influential in the overturning analysis. Angular velocity components

$\dot{\Phi}$ and $\dot{\Theta}$ in (10), on the other hand, are a simple consequence of the geometrical properties of the terrain.

If the terrain has mild slope gradients or the manipulator traverses the terrain with low velocity when slope gradients are significant, as already assumed, the contribution of terms $\dot{\Phi}$ and $\dot{\Theta}$ in the analysis of the forces can be neglected.

Assumption 4: The terrain itself and how the manipulator traverses uneven terrain does not significantly affect the angular velocity components of the chassis.

Corollary 4: Angular velocity components $\dot{\Phi}$ and $\dot{\Theta}$ are significantly smaller and less influential than the steering angular velocity $\dot{\Psi}$ and thus can be neglected, causing the following expression to hold approximately:

$$ {}^{\mathbf{B_C}}_{\mathbf{G}}\boldsymbol{\omega}_{\mathbf{B_C}} = \begin{pmatrix} 0 & 0 & \dot{\Psi} \end{pmatrix}^T. \tag{11} $$

Equation (11) follows from (10), based on Assumption 4. Assumptions 1 - 4 provide a basis for formulating the kinematics and dynamics relations. In the following discussion, subscripts FL, FR, RR, and RL will be used very often; these subscripts denote the **F**ront/**R**ear **L**eft/**R**ight (usually wheel).

Let us further consider the 4AWD platform from Fig. 3 which is the same manipulator wheeled platform as in Fig. 1, now shown in more detail, including wheels. The terms chassis and wheeled platform may be used interchangeably.

The wheeled platform's COM is located at point C, which also acts as the origin of the right-handed frame $\{\mathbf{B_C}\}$ with its x_{BC}-axis pointing in the longitudinal direction and with the y_{BC}-axis pointing in the lateral direction of the chassis motion. The position of each wheel with respect to the COM is determined with the set of 6 fixed lengths, labelled as l_1, l_2, and w_i, $i = \mathrm{FL, FR, RR, RL}$. Fig. 4 shows a mobile manipulator's simple oriented graph (SOG). The SOG in Fig. 4 shows that systematic kinematics calculations start from the velocity of the chassis COM and then branch towards wheels and manipulator TCP on the manipulator arm.

In the considered case of the platform's planar motion, as a consequence of Assumption 4, the chassis will presumably have velocity components only in the local level-ground plane. Each wheel's linear velocity can be calculated by knowing the magnitude and direction of the linear velocity of the chassis. Let the vector of the chassis COM linear velocities, with respect to the inertial frame of reference, and expressed as would be measured in the local chassis frame $\{\mathbf{B_C}\}$, be the following:

$$ {}^{\mathbf{B_C}}_{\mathbf{G}}\boldsymbol{v}_{\mathbf{B_C}} = \begin{pmatrix} V_C\ \cos\beta_C \\ V_C\ \sin\beta_C \\ 0 \end{pmatrix} = \begin{pmatrix} {}^{\mathbf{B_C}}v_{\mathrm{x}} \\ {}^{\mathbf{B_C}}v_{\mathrm{y}} \\ 0 \end{pmatrix}, \tag{12} $$

where V_C denotes the magnitude of the chassis COM velocity, and β_C denotes the instantaneous velocity angle of the chassis. If the angular velocity of the chassis is determined with (11), then by knowing values for ${}^{\mathbf{B_C}}v_{\mathrm{x}}$, ${}^{\mathbf{B_C}}v_{\mathrm{y}}$ and $\dot{\Psi}$, the magnitudes of all the wheel-related V_i, $i = \mathrm{FL, FR, RR, RL}$ and auxiliary $i = \mathrm{F, R}$ velocities can be calculated as [43] follows:

$$ V_{\mathrm{FL}}\ \sin\beta_{\mathrm{FL}} = V_C\ \sin\beta_C + l_2\,\dot{\Psi}, \tag{13} $$

$$ V_{\mathrm{FL}}\ \cos\beta_{\mathrm{FL}} = V_C\ \cos\beta_C - w_{\mathrm{FL}}\,\dot{\Psi}, \tag{14} $$

$$ V_{\mathrm{FR}}\ \sin\beta_{\mathrm{FR}} = V_C\ \sin\beta_C + l_2\,\dot{\Psi}, \tag{15} $$

$$ V_{\mathrm{FR}}\ \cos\beta_{\mathrm{FR}} = V_C\ \cos\beta_C + w_{\mathrm{FR}}\,\dot{\Psi}, \tag{16} $$

$$ V_{\mathrm{RR}}\ \sin\beta_{\mathrm{RR}} = V_C\ \sin\beta_C - l_1\,\dot{\Psi}, \tag{17} $$

$$ V_{\mathrm{RR}}\ \cos\beta_{\mathrm{RR}} = V_C\ \cos\beta_C + w_{\mathrm{RR}}\,\dot{\Psi}, \tag{18} $$

$$ V_{\mathrm{RL}}\ \sin\beta_{\mathrm{RL}} = V_C\ \sin\beta_C - l_1\,\dot{\Psi}, \tag{19} $$

$$ V_{\mathrm{RL}}\ \cos\beta_{\mathrm{RL}} = V_C\ \cos\beta_C - w_{\mathrm{RL}}\,\dot{\Psi}, \tag{20} $$

$$ V_F\ \sin\beta_F = V_C\ \sin\beta_C + l_2\,\dot{\Psi}, \tag{21} $$

$$ V_F\ \cos\beta_F = V_C\ \cos\beta_C, \tag{22} $$

$$ V_R\ \sin\beta_R = V_C\ \sin\beta_C - l_1\,\dot{\Psi}, \tag{23} $$

$$ V_F\ \cos\beta_R = V_C\ \cos\beta_R, \tag{24} $$

where the instantaneous velocity direction angles β_i, $i = \mathrm{FL, FR, RR, RL, F, R}$ are determined as follows:

$$ \beta_{\mathrm{FL}} = \arctan\frac{V_C\ \sin\beta_C + l_2\,\dot{\Psi}}{V_C\ \cos\beta_C - w_{\mathrm{FL}}\,\dot{\Psi}}, \tag{25} $$

$$ \beta_{\mathrm{FR}} = \arctan\frac{V_C\ \sin\beta_C + l_2\,\dot{\Psi}}{V_C\ \cos\beta_C + w_{\mathrm{FR}}\,\dot{\Psi}}, \tag{26} $$

$$ \beta_{\mathrm{RR}} = \arctan\frac{V_C\ \sin\beta_C - l_1\,\dot{\Psi}}{V_C\ \cos\beta_C + w_{\mathrm{RR}}\,\dot{\Psi}}, \tag{27} $$

$$ \beta_{\mathrm{RL}} = \arctan\frac{V_C\ \sin\beta_C - l_1\,\dot{\Psi}}{V_C\ \cos\beta_C - w_{\mathrm{RL}}\,\dot{\Psi}}, \tag{28} $$

$$ \beta_F = \arctan\frac{V_C\ \sin\beta_C + l_2\,\dot{\Psi}}{V_C\ \cos\beta_C}, \tag{29} $$

$$ \beta_R = \arctan\frac{V_C\ \sin\beta_C - l_1\,\dot{\Psi}}{V_C\ \cos\beta_C}. \tag{30} $$

By having all the instantaneous velocity angles β_i, the tyre and auxiliary sideslip angles can be calculated, if the wheel and auxiliary steering angles δ_i are known, as follows:

$$ \alpha_i = \beta_i - \delta_i, \quad i = \mathrm{FL, FR, RR, RL, F, R}. \tag{31} $$

Kinematic relations in a manipulator arm have to be established from case to case, and thus, no general approach can be presented here. However, it is clear that in the formation of a kinematics chain of the manipulator arm, the starting point will be the chassis, with the TCP at the end of the chain.

VI. 6D VECTOR MOBILE MANIPULATOR DYNAMICS

A. WHEEL DYNAMICS

The vehicle dynamics are mainly affected by the tyre/road interaction, that is, by forces and moments generated under the tyres. These forces and moments are usually modelled by combining empirical and theoretical approaches. The appropriate planes and frames in which the tyre/road interactions will be expressed and quantified are introduced and are shown in Fig. 5. The wheel-centre plane (wcp) contains a flat disk obtained by narrowing the tyre, whereas the vertical plane (vp) is always normal to the ground plane (gp), [44].

The center of the i-th tyre frame $\{\mathbf{T}_i\}$, $i = \mathrm{FL, FR, RR, RL}$, is at the centre of the tyreprint. The tyreprint is assumed to be at the wheel-centre plane and the ground plane intersection.

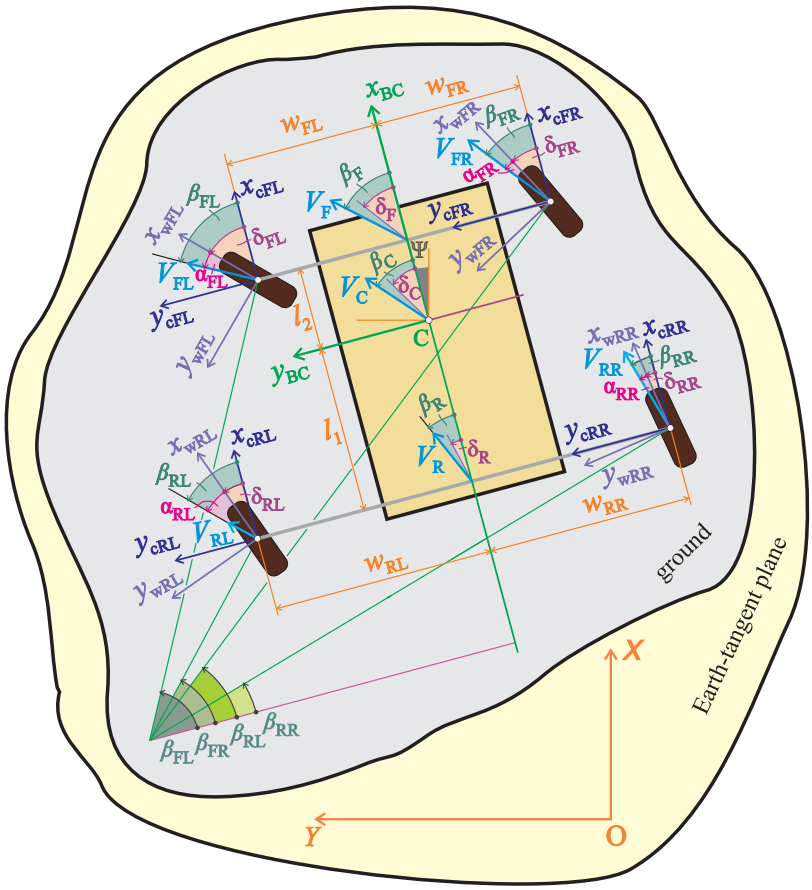

FIGURE 3. A wheeled manipulator platform when negotiating a slope, with all the relevant quantities in the kinematic analysis shown.

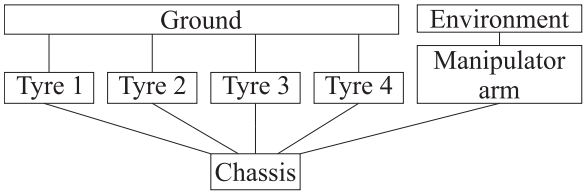

FIGURE 4. Simple oriented graph of the analysed mobile manipulator.

It follows the wheel's orientation, with its z_{ti}-axis always in the vertical plane. The wheel frame $\{\mathbf{W}_i\}$ has its origin at the wheel centre, where the COM is also assumed to be located. It will be chosen to move together with the wheel, except the spinning, because this benefits the dynamics analysis.

Although the wheel dynamics analysis benefits from using the non-spinning frame, [45], this does not allow the straightforward use of existing ready-to-use 6D dynamics equations as in the, for example, VDC mainstream form, where it is assumed that each body frame adopts all body motions.

The i-th wheel from Fig. 5 has its COM velocity vector laying in the plane parallel to the ground plane, which implies the following:

$$ {}^{\mathbf{T}_i}\boldsymbol{v}_i = \begin{pmatrix} V_i \cos\alpha_i \\ V_i \sin\alpha_i \\ 0 \end{pmatrix}, \tag{32} $$

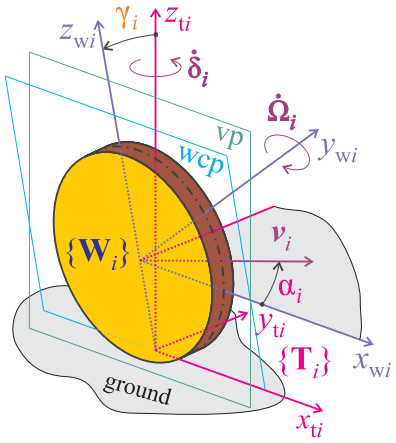

FIGURE 5. Wheel, with all the relevant planes, frames, axes and angles.

which can be expressed in the i-th wheel frame $\{\mathbf{W}_i\}$, using the sideslip angle α_i and the camber angle γ_i as follows:

$$ {}^{\mathbf{W}_i}\boldsymbol{v}_i = \begin{pmatrix} V_i \cos\alpha_i \\ V_i \sin\alpha_i \cos\gamma_i \\ -V_i \sin\alpha_i \sin\gamma_i \end{pmatrix}. \tag{33} $$

In (32) and (33), kinematic relations (12) - (31) are to be consulted. The i-th wheel, considered independently from the

vehicle, has the $\dot{\Omega}_i$ angular velocity component about the y_{wi}-axis and the $\dot{\delta}_i$ component about the z_{ti}-axis. Note that each wheel, considered as a part of a vehicle in the later analysis, will, in addition to these angular velocity components, adopt the angular velocity of the chassis and the term ${}^{\mathbf{W}_i}_{\mathbf{G}}\boldsymbol{\omega}_{\mathbf{B_C}}$ quantifies this, which seems to be often neglected or overlooked. Referring to Fig. 5, the angular velocity vector of the i-th wheel can be expressed in the i-th non-spinning wheel frame $\{\mathbf{W}_i\}$ as follows:

$$ {}^{\mathbf{W}_i}\boldsymbol{\omega}_i = \begin{pmatrix} 0 \\ \dot{\Omega}_i + \dot{\delta}_i \sin\gamma_i \\ \dot{\delta}_i \cos\gamma_i \end{pmatrix} + {}^{\mathbf{W}_i}_{\mathbf{G}}\boldsymbol{\omega}_{\mathbf{B_C}}. \tag{34} $$

As is already mentioned, because for the frame $\{\mathbf{W}_i\}$, we choose not to adopt the wheel's spinning motion, quantified by $\dot{\Omega}_i$, the angular velocity of the i-th wheel frame $\{\mathbf{W}_i\}$ *per se* is given as follows:

$$ {}^{\mathbf{W}_i}\boldsymbol{\omega}_{\mathbf{W}_i} = \begin{pmatrix} 0 \\ \dot{\delta}_i \sin\gamma_i \\ \dot{\delta}_i \cos\gamma_i \end{pmatrix} + {}^{\mathbf{W}_i}_{\mathbf{G}}\boldsymbol{\omega}_{\mathbf{B_C}}. \tag{35} $$

The change of linear momentum of the i-th wheel, expressed in the wheel frame $\{\mathbf{W}_i\}$, can be written as follows:

$$ m_i\,{}^{\mathbf{W}_i}\dot{\boldsymbol{v}}_i + m_i \left({}^{\mathbf{W}_i}\boldsymbol{\omega}_{\mathbf{W}_i}\times\right) {}^{\mathbf{W}_i}\boldsymbol{v}_i + m_i\,{}^{\mathbf{W}_i}\boldsymbol{g} = {}^{\mathbf{W}_i}\boldsymbol{f}_{\boldsymbol{i}}^{*}, \tag{36} $$

with m_i denoting the mass of the i-th wheel, ${}^{\mathbf{W}_i}\boldsymbol{g} = \begin{pmatrix} 0 & 0 & g \end{pmatrix}^T$ being the gravity acceleration vector, and ${}^{\mathbf{W}_i}\boldsymbol{f}_{\boldsymbol{i}}^{*}$ representing the total force vector acting on the i-th wheel, both expressed as would be measured in the $\{\mathbf{W}_i\}$ frame. The remaining equations required to describe the wheel motion give the angular momentum change as follows:

$$ \left[{}^{\mathbf{W}_i}\mathbf{I}\right] {}^{\mathbf{W}_i}\dot{\boldsymbol{\omega}}_i + \left({}^{\mathbf{W}_i}\boldsymbol{\omega}_{\mathbf{W}_i}\times\right) \left(\left[{}^{\mathbf{W}_i}\mathbf{I}\right] {}^{\mathbf{W}_i}\boldsymbol{\omega}_i\right) = {}^{\mathbf{W}_i}\boldsymbol{m}_{\boldsymbol{i}}^{*}, \tag{37} $$

with $\left[{}^{\mathbf{W}_i}\mathbf{I}\right]$ representing the inertia tensor of the i-th wheel about the $\{\mathbf{W}_i\}$ frame axes and ${}^{\mathbf{W}_i}\boldsymbol{m}_{\boldsymbol{i}}^{*}$ representing the total external moment vector acting on the i-th wheel, expressed as would be measured in the $\{\mathbf{W}_i\}$ frame. We note that in both (36) and (37), the frame angular velocity exists given per (35), whereas (34) participates only in (37).

At this point, the 6D dynamics model can be formed. The translational and rotational i-th wheel dynamics are thus described per (36) and (37). By introducing the 6D linear/angular velocity vector ${}^{\mathbf{W}_i}\boldsymbol{V}_i$ per (33) and (34) as follows:

$$ {}^{\mathbf{W}_i}\boldsymbol{V}_i = \begin{pmatrix} {}^{\mathbf{W}_i}\boldsymbol{v}_i \\ {}^{\mathbf{W}_i}\boldsymbol{\omega}_i \end{pmatrix}, \tag{38} $$

the 6D wheel/tyre dynamics equations can be given in the compact form:

$$ \mathbf{M}_{\mathbf{W}_i}\,{}^{\mathbf{W}_i}\dot{\boldsymbol{V}}_i + \mathbf{C}_{\mathbf{W}_i}\,{}^{\mathbf{W}_i}\boldsymbol{V}_i + \mathbf{G}_{\mathbf{W}_i} = {}^{\mathbf{W}_i}\boldsymbol{F}^{*}, \tag{39} $$

with matrices $\mathbf{M}_{\mathbf{W}_i}$, $\mathbf{C}_{\mathbf{W}_i}$ and the vector $\mathbf{G}_{\mathbf{W}_i}$ being:

$$ \mathbf{M}_{\mathbf{W}_i} = \begin{pmatrix} m_i\,\mathbf{I}_{3\times3} & \mathbf{O}_{3\times3} \\ \mathbf{O}_{3\times3} & \left[{}^{\mathbf{W}_i}\mathbf{I}\right] \end{pmatrix}, \tag{40} $$

$$ \mathbf{C}_{\mathbf{W}_i} = \begin{pmatrix} m_i \left({}^{\mathbf{W}_i}\boldsymbol{\omega}_{\mathbf{W}_i}\times\right) & \mathbf{O}_{3\times3} \\ \mathbf{O}_{3\times3} & \left({}^{\mathbf{W}_i}\boldsymbol{\omega}_{\mathbf{W}_i}\times\right) \left[{}^{\mathbf{W}_i}\mathbf{I}\right] \end{pmatrix}, \tag{41} $$

$$ \mathbf{G}_{\mathbf{W}_i} = \begin{pmatrix} m_i\,{}^{\mathbf{W}_i}\boldsymbol{g} \\ \mathbf{0}_{3\times1} \end{pmatrix}. \tag{42} $$

The inertia matrix $\mathbf{M}_{\mathbf{W}_i}$ remains symmetric here, as when the body frame adopts all body motions. Notably, matrix $\mathbf{C}_{\mathbf{W}_i}$ is now not anti-symmetric in general.

B. WHEEL/CHASSIS INTERACTION

The next topic requiring attention is the interaction between the wheel and chassis per the modelling modularity property and appending on the wheel/tyre subsystem dynamics analysis. If the aerodynamic forces acting on the wheel itself are neglected, the essential and unavoidable external forces/moments to be accounted for will undoubtedly remain the tyre/road interaction forces/moments ${}^{\mathbf{T}_i}\boldsymbol{F}$, the wheel actuation and joint friction moments ${}^{\mathbf{W}_i}\boldsymbol{F}_a$ and the wheel/chassis interaction forces/moments ${}^{\mathbf{W}_i}\boldsymbol{\eta}_i$.

By referring to Fig. 6 for providing graphical insights, the total force acting on each wheel, i.e. the right-hand side of (39), can be written as the following sum:

$$ {}^{\mathbf{W}_i}\boldsymbol{F}^{*} = -{}^{\mathbf{W}_i}\boldsymbol{\eta}_i + {}^{\mathbf{W}_i}\mathbf{U}_{\mathbf{T}_i}\,{}^{\mathbf{T}_i}\boldsymbol{F} + {}^{\mathbf{W}_i}\boldsymbol{F}_a, \tag{43} $$

with i = FL, FR, RR, RL in the case considered here. Once the wheel inertial forces and the forces formed at the tyreprint centre are known, the wheel/chassis interaction force vector ${}^{\mathbf{W}_i}\boldsymbol{\eta}_i$, which will directly actuate the chassis, can be calculated as follows:

$$ {}^{\mathbf{W}_i}\boldsymbol{\eta}_i = -{}^{\mathbf{W}_i}\boldsymbol{F}^{*} + {}^{\mathbf{W}_i}\mathbf{U}_{\mathbf{T}_i}\,{}^{\mathbf{T}_i}\boldsymbol{F} + {}^{\mathbf{W}_i}\boldsymbol{F}_a, \tag{44} $$

with i = FL, FR, RR, RL.

Even in the general case with n wheels, each wheel's dynamics could be given with (39), where the total force acting on each wheel is (43). Beginning the analysis from a manipulator with n wheels and with articulated steering would undoubtedly cause derivations of all the underlying expressions to be filled with numerous terms that could divert attention from the essence.

C. CHASSIS DYNAMICS

We now focus on the chassis of the considered 4AWD vehicle in Fig. 6. The chassis dynamics, in this case, can be easily described, assuming that the frame $\{\mathbf{B_C}\}$ adopts all the chassis motions.

The total force acting on the chassis is given as follows:

$$ \mathbf{M}_{\mathbf{B_C}}\,{}^{\mathbf{B_C}}\dot{\boldsymbol{V}} + \mathbf{C}_{\mathbf{B_C}}\,{}^{\mathbf{B_C}}\boldsymbol{V} + \mathbf{G}_{\mathbf{B_C}} = {}^{\mathbf{B_C}}\boldsymbol{F}^{*}, \tag{45} $$

where the detailed expressions for matrices $\mathbf{M}_{\mathbf{B_C}}$, $\mathbf{C}_{\mathbf{B_C}}$ and $\mathbf{G}_{\mathbf{B_C}}$ are the same as in [38]. The total force acting on the chassis can be equivalently represented by the following sum:

$$ {}^{\mathbf{B_C}}\boldsymbol{F}^{*} = {}^{\mathbf{B_C}}\mathbf{U}_{\mathbf{B_M}}\,{}^{\mathbf{B_M}}\boldsymbol{F} + \sum_{i=\mathrm{FL},\ldots,\mathrm{RL}} {}^{\mathbf{B_C}}\mathbf{U}_{\mathbf{W}_i}\,{}^{\mathbf{W}_i}\boldsymbol{\eta}_i, \tag{46} $$

where ${}^{\mathbf{B_M}}\boldsymbol{F}$ represents the manipulator base reaction force, and ${}^{\mathbf{W}_i}\boldsymbol{\eta}$ represents the wheel/chassis interaction expressed

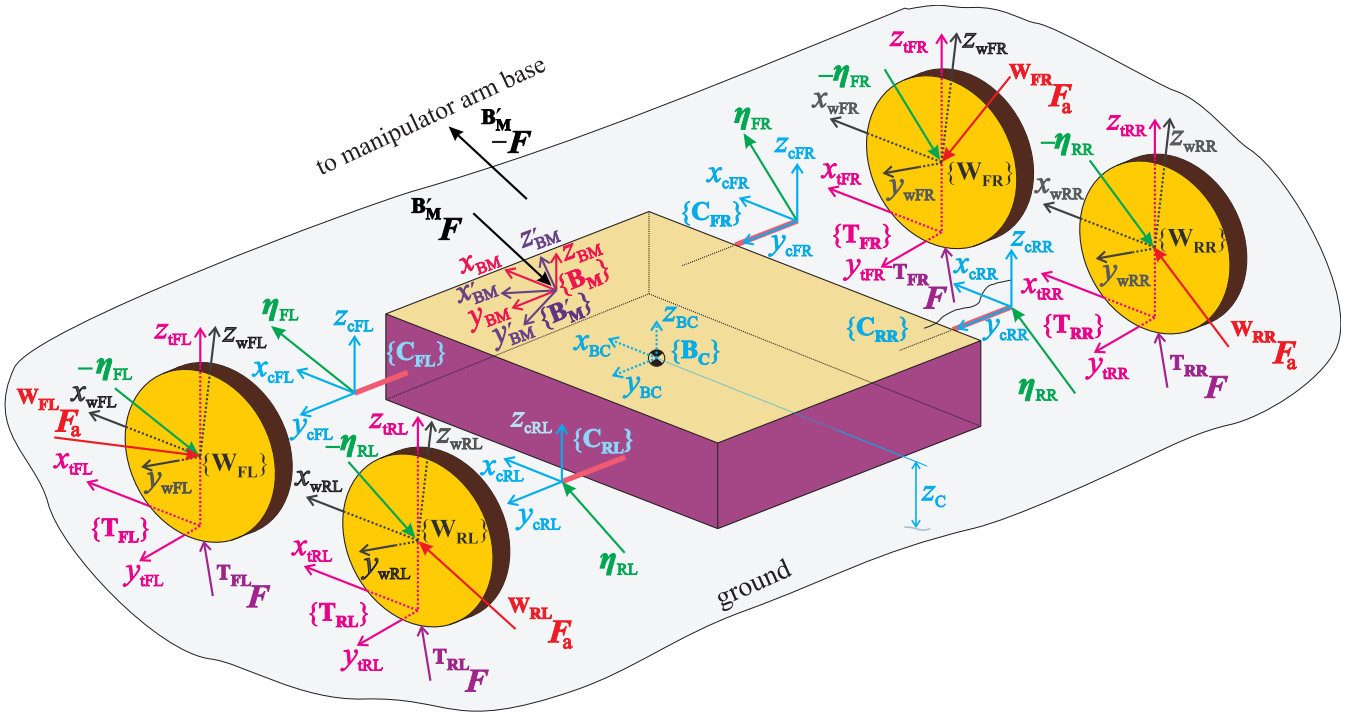

FIGURE 6. Free body diagram of the chassis and wheels. Ground reactions are smoothly included in the analysis when using the N–E formalism.

as would be measured in the $\{\mathbf{W}_i\}$ frame. All the existing tipping-over criteria have been derived assuming that in (44), terms ${}^{\mathbf{W}_i}\boldsymbol{F}^*$ and ${}^{\mathbf{W}_i}\boldsymbol{F}_a$ are equal to zero. While the MHS assumed that the left-hand side of (45) equals zero, the TMO considers only the $\mathbf{G}_{\mathbf{B_C}}$ term, and the ITMO uses the complete left-hand side of (45) as given here.

VII. WEIGHT TRANSFER TO MANIPULATOR WHEELS

In the derivation process of MHS, TOM and ITOM, at this modelling stage, with underlying assumptions being valid, the moments about the axes connecting the supporting polygon vertices have been formed, and no further steps are taken towards the analytical determination of the supporting forces.

As a consequence of Assumption 3, the forces supporting the wheel only affect the linear motion in the direction of their action and angular motions about axes in the plane parallel to the level-ground plane, i.e. pitching and rolling angular motion. Consequently, when we have only three equations, the challenge in the process of determining the forces is that there are fewer equations than unknown variables in the case of four or more wheels. Additional reasonable relations for connecting the tyre loads are then introduced to obtain the closed-form system of equations, as in [46], or the solution is found using a matrix pseudoinverse.

Before proceeding further, the wheel forces and moments must be addressed since it may simplify the following analysis. When performing dynamics analysis at the wheel level, the wheel's inertial forces are critical for predicting the wheel's motion. In contrast, neglecting the wheel's inertial forces could lead to much simpler final expressions without introducing significant modelling errors when calculating the normal loads. Let us take, for example, a moving mobile manipulator which accelerates. If the chassis mass is a few times the mass of the wheels, then its contribution to the inertial forces of the system is dominant. In the case of a manipulator moving at low to zero velocities during the working tasks, even the inertial forces of the chassis are certainly negligible because accelerations of the manipulator arm are the ones having significant velocities and accelerations. These considerations motivate the neglection of the wheel inertial forces for each wheel. If this neglection may not be valid in the particular case, the full-dynamics model presented here extends results to any desired extent.

Accounting for the weight of wheels will not make the normal force expressions significantly complex and could be a significant factor, especially when big heavy wheels of heavy-duty machines at low velocities are being considered.

Assumption 5: Inertial forces of all the wheels are negligible with respect to the chassis inertial forces.

Corollary 5: Inertial forces of each wheel and all wheel actuation torques are neglected, leaving only the respective wheel weights to be considered when calculating normal loads. In the normal load analysis, the wheel/chassis interaction force will have the following form:

$$ {}^{\mathbf{W}_i}\boldsymbol{\eta}_i = -\mathbf{G}_{\mathbf{W}_i} + {}^{\mathbf{W}_i}\mathbf{U}_{\mathbf{T}_i}\,{}^{\mathbf{T}_i}\boldsymbol{F}, \tag{47} $$

with ${}^{\mathbf{T}_i}\boldsymbol{F} = \left({}^{\mathbf{T}_i}f_x \;\; {}^{\mathbf{T}_i}f_y \;\; {}^{\mathbf{T}_i}f_z \;\; 0 \;\; 0 \;\; 0\right)^T$.

To avoid more complicated notations in the following expressions, additional reasonable assumptions on the wheels, which are commonly understood in such analyses, are applied here. If some of these may not hold in a specific case, a more general result can be obtained following the presented procedure. Here, it is assumed that:

Assumption 6: All the wheels are nominally equal, having zero camber angles, same masses, same radii, and same lateral distances from the chassis COM.

Corollary 6: All the wheel distances from the chassis w_i, wheel masses $m_{\mathrm{w}i}$ and wheel radii $R_{\mathrm{w}i}$ have equal values, which are labelled as w, m_{w} and R_{w}, respectively, with camber angles $\gamma_i = 0$, where $i =$ FL, FR, RR, RL.

The three equations of motion in which normal loads participate follow from a combination of (45) and (46), and these are (48)–(50), as shown at the bottom of the page. Combining them with (51) and (52), as shown at the bottom of the page, provides three equations with four unknown normal loads ${}^{\mathbf{T}_{\mathbf{FL}}}f_z$, ${}^{\mathbf{T}_{\mathbf{FR}}}f_z$, ${}^{\mathbf{T}_{\mathbf{RR}}}f_z$, ${}^{\mathbf{T}_{\mathbf{RL}}}f_z$. Auxiliary vectors used in (48) – (52) are $\mathbf{x}_f = \begin{pmatrix}1&0&0&0&0&0\end{pmatrix}^T$, $\mathbf{y}_f = \begin{pmatrix}0&1&0&0&0&0\end{pmatrix}^T$, $\mathbf{z}_f = \begin{pmatrix}0&0&1&0&0&0\end{pmatrix}^T$, $\mathbf{x}_\tau = \begin{pmatrix}0&0&0&1&0&0\end{pmatrix}^T$, $\mathbf{y}_\tau = \begin{pmatrix}0&0&0&0&1&0\end{pmatrix}^T$.

Before presenting the main result, it is vital to address how the base frame of the manipulator arm is oriented to the frame $\{\mathbf{B_C}\}$ at the chassis COM. The mutual orientation of these frames will, of course, affect the final expressions for the normal wheel loads. In the general case, this orientation can be any, and if it were to be accounted for directly, many additional terms in final expressions coming from the rotation matrix coefficients would appear. For the sake of analysis clarity, it is convenient to have both the manipulator arm base $\{\mathbf{B'_M}\}$ frame, which adopts all the manipulator base motions, and frame $\{\mathbf{B_M}\}$ with the same origin as $\{\mathbf{B'_M}\}$, but with the same orientation as $\{\mathbf{B_C}\}$, per Fig. 6. By doing so, the generality of the model is retained while ready-to-use expressions for normal loads are derived and presented as simply as possible. The considerations above that are introduced simply for the convenience of presentation lead to the assumption:

Assumption 7: Frame $\{\mathbf{B_M}\}$ at the connection of the manipulator arm base and the chassis has the same orientation as that of frame $\{\mathbf{B_C}\}$ at the chassis COM.

Corollary 7: The rotation matrix from frame $\{\mathbf{B_C}\}$ to the frame $\{\mathbf{B_M}\}$ is an identity matrix ${}^{\mathbf{B_M}}\mathbf{R}_{\mathbf{B_C}} = \mathbf{I}_{3\times3}$.

The main implication of Assumption 7 is that an inevitable and insignificant burden is placed on the end-user to calculate ${}^{\mathbf{B_M}}\boldsymbol{F}$ before using the main results. If the equations derived below are to be used directly, one must transform the forces/moments from frame $\{\mathbf{B'_M}\}$ to frame $\{\mathbf{B_M}\}$ as:

$$ {}^{\mathbf{B_M}}\boldsymbol{F} = {}^{\mathbf{B_M}}\mathbf{U}_{\mathbf{B'_M}}\, {}^{\mathbf{B'_M}}\boldsymbol{F}. \tag{53} $$

Forces/moments vector ${}^{\mathbf{B'_M}}\boldsymbol{F}$ at the manipulator arm base can be calculated as, for example, in [37], can be easily obtained by knowing the orientation of the manipulator

$$ \mathbf{z}_f \left({}^{\mathbf{B_C}}\mathbf{U}_{\mathbf{B_M}}\, {}^{\mathbf{B_M}}\boldsymbol{F} + \sum_{i=\mathrm{FL,FR,RR,RL}} {}^{\mathbf{B_C}}\mathbf{U}_{\mathbf{W}_i}\, {}^{\mathbf{W}_i}\boldsymbol{\eta}_i \right) = \mathbf{z}_f \left(\mathbf{M}_{\mathbf{B_C}}\, {}^{\mathbf{B_C}}\dot{\boldsymbol{V}} + \mathbf{C}_{\mathbf{B_C}}\, {}^{\mathbf{B_C}}\boldsymbol{V} + \mathbf{G}_{\mathbf{B_C}} \right) $$
$$ = m_{\mathrm{BC}}\, g \tag{48} $$

$$ \mathbf{x}_\tau \left({}^{\mathbf{B_C}}\mathbf{U}_{\mathbf{B_M}}\, {}^{\mathbf{B_M}}\boldsymbol{F} + \sum_{i=\mathrm{FL,FR,RR,RL}} {}^{\mathbf{B_C}}\mathbf{U}_{\mathbf{W}_i}\, {}^{\mathbf{W}_i}\boldsymbol{\eta}_i \right) = \mathbf{x}_\tau \left(\mathbf{M}_{\mathbf{B_C}}\, {}^{\mathbf{B_C}}\dot{\boldsymbol{V}} + \mathbf{C}_{\mathbf{B_C}}\, {}^{\mathbf{B_C}}\boldsymbol{V} + \mathbf{G}_{\mathbf{B_C}} \right) $$
$$ = -{}^{\mathbf{B_C}}I_{\mathrm{xy}}\, \dot{\Psi}^2 + {}^{\mathbf{B_C}}I_{\mathrm{xz}}\, \ddot{\Psi} \tag{49} $$

$$ \mathbf{y}_\tau \left({}^{\mathbf{B_C}}\mathbf{U}_{\mathbf{B_M}}\, {}^{\mathbf{B_M}}\boldsymbol{F} + \sum_{i=\mathrm{FL,FR,RR,RL}} {}^{\mathbf{B_C}}\mathbf{U}_{\mathbf{W}_i}\, {}^{\mathbf{W}_i}\boldsymbol{\eta}_i \right) = \mathbf{y}_\tau \left(\mathbf{M}_{\mathbf{B_C}}\, {}^{\mathbf{B_C}}\dot{\boldsymbol{V}} + \mathbf{C}_{\mathbf{B_C}}\, {}^{\mathbf{B_C}}\boldsymbol{V} + \mathbf{G}_{\mathbf{B_C}} \right) $$
$$ = -{}^{\mathbf{B_C}}I_{\mathrm{xz}}\, \dot{\Psi}^2 + {}^{\mathbf{B_C}}I_{\mathrm{yz}}\, \ddot{\Psi} \tag{50} $$

$$ \mathbf{x}_f \left({}^{\mathbf{B_C}}\mathbf{U}_{\mathbf{B_M}}\, {}^{\mathbf{B_M}}\boldsymbol{F} + \sum_{i=\mathrm{FL,FR,RR,RL}} {}^{\mathbf{B_C}}\mathbf{U}_{\mathbf{W}_i}\, {}^{\mathbf{W}_i}\boldsymbol{\eta}_i \right) = \mathbf{x}_f \left(\mathbf{M}_{\mathbf{B_C}}\, {}^{\mathbf{B_C}}\dot{\boldsymbol{V}} + \mathbf{C}_{\mathbf{B_C}}\, {}^{\mathbf{B_C}}\boldsymbol{V} + \mathbf{G}_{\mathbf{B_C}} \right) $$
$$ = m_{\mathrm{BC}} \left({}^{\mathbf{B_C}}\dot{v}_{\mathrm{y}} + {}^{\mathbf{B_C}}v_{\mathrm{x}}\, \dot{\Psi} \right) \tag{51} $$

$$ \mathbf{y}_f \left({}^{\mathbf{B_C}}\mathbf{U}_{\mathbf{B_M}}\, {}^{\mathbf{B_M}}\boldsymbol{F} + \sum_{i=\mathrm{FL,FR,RR,RL}} {}^{\mathbf{B_C}}\mathbf{U}_{\mathbf{W}_i}\, {}^{\mathbf{W}_i}\boldsymbol{\eta}_i \right) = \mathbf{y}_f \left(\mathbf{M}_{\mathbf{B_C}}\, {}^{\mathbf{B_C}}\dot{\boldsymbol{V}} + \mathbf{C}_{\mathbf{B_C}}\, {}^{\mathbf{B_C}}\boldsymbol{V} + \mathbf{G}_{\mathbf{B_C}} \right) $$
$$ = m_{BC} \left({}^{\mathbf{B_C}}\dot{v}_{\mathrm{x}} - {}^{\mathbf{B_C}}v_{\mathrm{y}}\, \dot{\Psi} \right) \tag{52} $$

arm base frame $\{\mathbf{B}'_{\mathbf{M}}\}$ with respect to the chassis-fixed frame $\{\mathbf{B_M}\}$.

If the solution obtained using the pseudoinversion is to be avoided, a unique solution for the supporting forces can be obtained by introducing a suspension-related assumption. It connects the normal load differences on the front and rear axle. Following the vehicle dynamics modelling principles, we introduce

Assumption 8 [46]: The lateral load difference across the front axle is some fraction of the total lateral load difference.

Corollary 8: The following equation is recognized:

$$^{\mathbf{TFR}}f_z - {}^{\mathbf{TFL}}f_z = D\left({}^{\mathbf{TFR}}f_z + {}^{\mathbf{TRR}}f_z - {}^{\mathbf{TFL}}f_z - {}^{\mathbf{TRL}}f_z\right), \quad (54)$$

with $D \in [0, 1]$.

The final system of equations for the normal load calculation with $D = 0.5$ in (54) is given as follows:

$$\begin{pmatrix} w & -w & -w & w \\ -l_2 & -l_2 & l_1 & l_1 \\ 1 & 1 & 1 & 1 \\ -0.5 & 0.5 & -0.5 & 0.5 \end{pmatrix} \begin{pmatrix} {}^{\mathbf{TFL}}f_z \\ {}^{\mathbf{TFR}}f_z \\ {}^{\mathbf{TRR}}f_z \\ {}^{\mathbf{TRL}}f_z \end{pmatrix} = \begin{pmatrix} b_1 \\ b_2 \\ b_3 \\ 0 \end{pmatrix}, \quad (55)$$

where the corresponding b_i from (55), $i = 1, 2, 3$ is:

Particular terms in (56)–(58), as shown at the bottom of the page, with the left superscript $\mathbf{B_M}$ arise from the existence of the forces/moments being built up at the connection of the chassis and the manipulator base. The vector ${}^{\mathbf{B_M}}\boldsymbol{F}$ is assumed to have the following structure:

$${}^{\mathbf{B_M}}\boldsymbol{F} = \begin{pmatrix} {}^{\mathbf{B_M}}f_{\mathrm{x}} \\ {}^{\mathbf{B_M}}f_{\mathrm{y}} \\ {}^{\mathbf{B_M}}f_{\mathrm{z}} \\ {}^{\mathbf{B_M}}m_{\mathrm{x}} \\ {}^{\mathbf{B_M}}m_{\mathrm{y}} \\ {}^{\mathbf{B_M}}m_{\mathrm{z}} \end{pmatrix}, \quad (59)$$

and thus the used notation in (56)–(58).

Further, the position vector of frame $\{\mathbf{B_M}\}$ with respect to frame $\{\mathbf{B_C}\}$, expressed in the $\{\mathbf{B_C}\}$ frame is as follows:

$${}^{\mathbf{B_C}}_{\mathbf{B_C}}\boldsymbol{r}_{\mathbf{B_M}} = \begin{pmatrix} x_{\mathrm{CA}} \\ y_{\mathrm{CA}} \\ z_{\mathrm{CA}} \end{pmatrix}, \quad (60)$$

and the components of this vector account explicitly for the placement of the manipulator arm base and how this placement affects the supporting forces.

The chassis tensor of inertia can be assumed to have a general form with no zero elements, where the chassis moments of inertia about the $\{\mathbf{B_C}\}$ frame axes are denoted by ${}^{\mathbf{B_C}}I_{\mathrm{ij}} = {}^{\mathbf{B_C}}I_{\mathrm{ji}}$, $i, j = \mathrm{x}, \mathrm{y}, \mathrm{z}$, and participate in (56)–(58).

In addition to the moments of inertia, the wheeled-platform mass has to be considered, and it is denoted by m_{BC}. The chassis COM height above the ground, a known contributing term, is labelled as z_C and is also sketched in Fig. 6.

The lengths l_1 and l_2 have been already introduced in Fig. 3 and are addressed in Section V. They represent distances from the chassis COM to the rear and front axle, respectively.

Finally, terms r_{ij}, where $i, j = 1, 2, 3$ are the ij-th coefficients of the transformation matrix (8), and it is these terms that account for the slope angles and thus for the chassis orientation with respect to the Earth-tangent plane.

By solving the system of equations (55), compact expressions for each tyre's supporting force can be obtained in the form of the following neat sums with eleven terms in each:

$${}^{\mathbf{TFL}}f_z = \sum_{i=1}^{11} \zeta_{\mathrm{FL},i}, \quad (61)$$

$${}^{\mathbf{TFR}}f_z = \sum_{i=1}^{11} \zeta_{\mathrm{FR},i}, \quad (62)$$

$${}^{\mathbf{TRR}}f_z = \sum_{i=1}^{11} \zeta_{\mathrm{RR},i}, \quad (63)$$

$${}^{\mathbf{TRL}}f_z = \sum_{i=1}^{11} \zeta_{\mathrm{RL},i}. \quad (64)$$

Analytic expressions for all the contributing terms in (61)–(64) are given by (65)–(108), [(65)–(68), as shown at the bottom of the next page]. Each term can be considered *static* if its contribution exists irrespective of the motion of the chassis or manipulator arm. Magnitudes of static terms are affected by the system masses, slope angles, manipulator arm posture, and the position of the connection point between the manipulator and the chassis. How the chassis and wheel weight forces contribute to the supporting forces is quantified with (65) – (68). In this case, slope angles are important contributors, together with the COM height.

Stato-dynamic terms (69) – (88) describe how the manipulator arm affects the normal loads. The location of the arm connection point with the chassis (60) plays an integral role in these terms. They can generally have non-zero static values,

$$\begin{aligned} b_1 = {} & (z_{\mathrm{CA}} + z_{\mathrm{C}})\, {}^{\mathbf{B_M}}f_{\mathrm{y}} - y_{\mathrm{CA}}\, {}^{\mathbf{B_M}}f_{\mathrm{z}} - {}^{\mathbf{B_M}}m_{\mathrm{x}} - g\,(m_{\mathrm{BC}}\, z_C + 4\, m_w\, R_w)\, r_{32} \\ & - m_{\mathrm{BC}}\, z_{\mathrm{C}} \left({}^{\mathbf{B_C}}\dot{v}_{\mathrm{y}} + {}^{\mathbf{B_C}}v_{\mathrm{x}}\, \dot{\Psi}\right) - {}^{\mathbf{B_C}}I_{\mathrm{yz}}\, \dot{\Psi}^2 + {}^{\mathbf{B_C}}I_{\mathrm{xz}}\, \ddot{\Psi}, \end{aligned} \quad (56)$$

$$\begin{aligned} b_2 = {} & -(z_{\mathrm{CA}} + z_{\mathrm{C}})\, {}^{\mathbf{B_M}}f_{\mathrm{x}} + x_{\mathrm{CA}}\, {}^{\mathbf{B_M}}f_{\mathrm{z}} - {}^{\mathbf{B_M}}m_{\mathrm{y}} + g\,(m_{\mathrm{BC}}\, z_C + 4\, m_w\, R_w)\, r_{31} \\ & + 2\, g\,(l_1 - l_2)\, m_w\, r_{33} + m_{\mathrm{BC}}\, z_C \left({}^{\mathbf{B_C}}\dot{v}_{\mathrm{x}} - {}^{\mathbf{B_C}}v_{\mathrm{y}}\, \dot{\Psi}\right) + {}^{\mathbf{B_C}}I_{\mathrm{xz}}\, \dot{\Psi}^2 + {}^{\mathbf{B_C}}I_{\mathrm{yz}}\, \ddot{\Psi}, \end{aligned} \quad (57)$$

$$b_3 = g\ (m_{\mathrm{BC}} + 4\, m_{\mathrm{w}})\ r_{33} - {}^{\mathbf{B_M}}f_{\mathrm{z}}. \quad (58)$$

which change when motion exists.

$$\zeta_{\mathrm{FL},2} = \frac{1}{2}\frac{z_{\mathrm{CA}} + z_{\mathrm{C}}}{l_1 + l_2}\,{}^{\mathbf{B_M}}f_{\mathrm{x}} \tag{69}$$

$$\zeta_{\mathrm{FR},2} = \frac{1}{2}\frac{z_{\mathrm{CA}} + z_{\mathrm{C}}}{l_1 + l_2}\,{}^{\mathbf{B_M}}f_{\mathrm{x}} \tag{70}$$

$$\zeta_{\mathrm{RR},2} = -\frac{1}{2}\frac{z_{\mathrm{CA}} + z_{\mathrm{C}}}{l_1 + l_2}\,{}^{\mathbf{B_M}}f_{\mathrm{x}} \tag{71}$$

$$\zeta_{\mathrm{RL},2} = -\frac{1}{2}\frac{z_{\mathrm{CA}} + z_{\mathrm{C}}}{l_1 + l_2}\,{}^{\mathbf{B_M}}f_{\mathrm{x}} \tag{72}$$

$$\zeta_{\mathrm{FL},3} = \frac{1}{4}\frac{z_{\mathrm{CA}} + z_{\mathrm{C}}}{w}\,{}^{\mathbf{B_M}}f_{\mathrm{y}} \tag{73}$$

$$\zeta_{\mathrm{FR},3} = -\frac{1}{4}\frac{z_{\mathrm{CA}} + z_{\mathrm{C}}}{w}\,{}^{\mathbf{B_M}}f_{\mathrm{y}} \tag{74}$$

$$\zeta_{\mathrm{RR},3} = -\frac{1}{4}\frac{z_{\mathrm{CA}} + z_{\mathrm{C}}}{w}\,{}^{\mathbf{B_M}}f_{\mathrm{y}} \tag{75}$$

$$\zeta_{\mathrm{RL},3} = \frac{1}{4}\frac{z_{\mathrm{CA}} + z_{\mathrm{C}}}{w}\,{}^{\mathbf{B_M}}f_{\mathrm{y}} \tag{76}$$

$$\zeta_{\mathrm{FL},4} = -\frac{1}{2}\left(\frac{l_1 + x_{\mathrm{CA}}}{l_1 + l_2} + \frac{1}{2}\frac{y_{\mathrm{CA}}}{w}\right){}^{\mathbf{B_M}}f_{\mathrm{z}} \tag{77}$$

$$\zeta_{\mathrm{FR},4} = -\frac{1}{2}\left(\frac{l_1 + x_{\mathrm{CA}}}{l_1 + l_2} - \frac{1}{2}\frac{y_{\mathrm{CA}}}{w}\right){}^{\mathbf{B_M}}f_{\mathrm{z}} \tag{78}$$

$$\zeta_{\mathrm{RR},4} = -\frac{1}{2}\left(\frac{l_2 - x_{\mathrm{CA}}}{l_1 + l_2} - \frac{1}{2}\frac{y_{\mathrm{CA}}}{w}\right){}^{\mathbf{B_M}}f_{\mathrm{z}} \tag{79}$$

$$\zeta_{\mathrm{RL},4} = -\frac{1}{2}\left(\frac{l_2 - x_{\mathrm{CA}}}{l_1 + l_2} + \frac{1}{2}\frac{y_{\mathrm{CA}}}{w}\right){}^{\mathbf{B_M}}f_{\mathrm{z}} \tag{80}$$

$$\zeta_{\mathrm{FL},5} = -\frac{{}^{\mathbf{B_M}}m_{\mathrm{x}}}{4\,w} \tag{81}$$

$$\zeta_{\mathrm{FR},5} = \frac{{}^{\mathbf{B_M}}m_{\mathrm{x}}}{4\,w} \tag{82}$$

$$\zeta_{\mathrm{RR},5} = \frac{{}^{\mathbf{B_M}}m_{\mathrm{x}}}{4\,w} \tag{83}$$

$$\zeta_{\mathrm{RL},5} = -\frac{{}^{\mathbf{B_M}}m_{\mathrm{x}}}{4\,w} \tag{84}$$

$$\zeta_{\mathrm{FL},6} = \frac{1}{2}\frac{{}^{\mathbf{B_M}}m_{\mathrm{y}}}{l_1 + l_2} \tag{85}$$

$$\zeta_{\mathrm{FR},6} = \frac{1}{2}\frac{{}^{\mathbf{B_M}}m_{\mathrm{y}}}{l_1 + l_2} \tag{86}$$

$$\zeta_{\mathrm{RR},6} = -\frac{1}{2}\frac{{}^{\mathbf{B_M}}m_{\mathrm{y}}}{l_1 + l_2} \tag{87}$$

$$\zeta_{\mathrm{RL},6} = -\frac{1}{2}\frac{{}^{\mathbf{B_M}}m_{\mathrm{y}}}{l_1 + l_2} \tag{88}$$

Terms (89) – (108) exist only when the wheeled platform is moving and thus can be addressed as *dynamic* terms. These provide insights into how the chassis linear/angular velocities and accelerations affect the normal wheel loads.

$$\zeta_{\mathrm{FL},7} = -\frac{m_{\mathrm{BC}}}{2}\frac{z_{\mathrm{C}}}{l_1 + l_2}\,{}^{\mathbf{B_C}}\dot{v}_{\mathrm{x}} \tag{89}$$

$$\zeta_{\mathrm{FR},7} = -\frac{m_{\mathrm{BC}}}{2}\frac{z_{\mathrm{C}}}{l_1 + l_2}\,{}^{\mathbf{B_C}}\dot{v}_{\mathrm{x}} \tag{90}$$

$$\zeta_{\mathrm{RR},7} = \frac{m_{\mathrm{BC}}}{2}\frac{z_{\mathrm{C}}}{l_1 + l_2}\,{}^{\mathbf{B_C}}\dot{v}_{\mathrm{x}} \tag{91}$$

$$\zeta_{\mathrm{RL},7} = \frac{m_{\mathrm{BC}}}{2}\frac{z_{\mathrm{C}}}{l_1 + l_2}\,{}^{\mathbf{B_C}}\dot{v}_{\mathrm{x}} \tag{92}$$

$$\zeta_{\mathrm{FL},8} = -\frac{m_{\mathrm{BC}}}{4}\frac{z_{\mathrm{C}}}{w}\,{}^{\mathbf{B_C}}\dot{v}_{\mathrm{y}} \tag{93}$$

$$\zeta_{\mathrm{FR},8} = \frac{m_{\mathrm{BC}}}{4}\frac{z_{\mathrm{C}}}{w}\,{}^{\mathbf{B_C}}\dot{v}_{\mathrm{y}} \tag{94}$$

$$\zeta_{\mathrm{RR},8} = \frac{m_{\mathrm{BC}}}{4}\frac{z_{\mathrm{C}}}{w}\,{}^{\mathbf{B_C}}\dot{v}_{\mathrm{y}} \tag{95}$$

$$\zeta_{\mathrm{RL},8} = -\frac{m_{\mathrm{BC}}}{4}\frac{z_{\mathrm{C}}}{w}\,{}^{\mathbf{B_C}}\dot{v}_{\mathrm{y}} \tag{96}$$

$$\zeta_{\mathrm{FL},9} = \frac{m_{\mathrm{BC}}}{2}\,z_{\mathrm{C}}\left(-\frac{{}^{\mathbf{B_C}}v_{\mathrm{x}}}{2\,w} + \frac{{}^{\mathbf{B_C}}v_{\mathrm{y}}}{l_1 + l_2}\right)\dot{\Psi} \tag{97}$$

$$\zeta_{\mathrm{FR},9} = \frac{m_{\mathrm{BC}}}{2}\,z_{\mathrm{C}}\left(\frac{{}^{\mathbf{B_C}}v_{\mathrm{x}}}{2\,w} + \frac{{}^{\mathbf{B_C}}v_{\mathrm{y}}}{l_1 + l_2}\right)\dot{\Psi} \tag{98}$$

$$\zeta_{\mathrm{RR},9} = -\frac{m_{\mathrm{BC}}}{2}\,z_{\mathrm{C}}\left(-\frac{{}^{\mathbf{B_C}}v_{\mathrm{x}}}{2\,w} + \frac{{}^{\mathbf{B_C}}v_{\mathrm{y}}}{l_1 + l_2}\right)\dot{\Psi} \tag{99}$$

$$\zeta_{\mathrm{RL},9} = -\frac{m_{\mathrm{BC}}}{2}\,z_{\mathrm{C}}\left(\frac{{}^{\mathbf{B_C}}v_{\mathrm{x}}}{2\,w} + \frac{{}^{\mathbf{B_C}}v_{\mathrm{y}}}{l_1 + l_2}\right)\dot{\Psi} \tag{100}$$

$$\zeta_{\mathrm{FL},10} = -\frac{1}{2}\left(\frac{{}^{\mathbf{B_C}}I_{\mathrm{xz}}}{l_1 + l_2} + \frac{{}^{\mathbf{B_C}}I_{\mathrm{yz}}}{2\,w}\right)\dot{\Psi}^2 \tag{101}$$

$$\zeta_{\mathrm{FR},10} = -\frac{1}{2}\left(\frac{{}^{\mathbf{B_C}}I_{\mathrm{xz}}}{l_1 + l_2} - \frac{{}^{\mathbf{B_C}}I_{\mathrm{yz}}}{2\,w}\right)\dot{\Psi}^2 \tag{102}$$

$$\zeta_{\mathrm{RR},10} = \frac{1}{2}\left(\frac{{}^{\mathbf{B_C}}I_{\mathrm{xz}}}{l_1 + l_2} + \frac{{}^{\mathbf{B_C}}I_{\mathrm{yz}}}{2\,w}\right)\dot{\Psi}^2 \tag{103}$$

$$\zeta_{\mathrm{RL},10} = \frac{1}{2}\left(\frac{{}^{\mathbf{B_C}}I_{\mathrm{xz}}}{l_1 + l_2} - \frac{{}^{\mathbf{B_C}}I_{\mathrm{yz}}}{2\,w}\right)\dot{\Psi}^2 \tag{104}$$

$$\zeta_{\mathrm{FL},1} = g\left(\frac{m_{\mathrm{BC}}}{2}\frac{l_1}{l_1 + l_2} + m_{\mathrm{w}}\right)r_{33} - \frac{g\,(m_w R_w + 0.25\,m_{\mathrm{BC}}\,z_C)}{w}\,r_{32} - \frac{2\,g\,(m_w R_w + 0.25\,m_{\mathrm{BC}}\,z_C)}{l_1 + l_2}\,r_{31} \tag{65}$$

$$\zeta_{\mathrm{FR},1} = g\left(\frac{m_{\mathrm{BC}}}{2}\frac{l_1}{l_1 + l_2} + m_{\mathrm{w}}\right)r_{33} + \frac{g\,(m_w R_w + 0.25\,m_{\mathrm{BC}}\,z_C)}{w}\,r_{32} - \frac{2\,g\,(m_w R_w + 0.25\,m_{\mathrm{BC}}\,z_C)}{l_1 + l_2}\,r_{31} \tag{66}$$

$$\zeta_{\mathrm{RR},1} = g\left(\frac{m_{\mathrm{BC}}}{2}\frac{l_2}{l_1 + l_2} + m_{\mathrm{w}}\right)r_{33} + \frac{g\,(m_w R_w + 0.25\,m_{\mathrm{BC}}\,z_C)}{w}\,r_{32} + \frac{2\,g\,(m_w R_w + 0.25\,m_{\mathrm{BC}}\,z_C)}{l_1 + l_2}\,r_{31} \tag{67}$$

$$\zeta_{\mathrm{RL},1} = g\left(\frac{m_{\mathrm{BC}}}{2}\frac{l_2}{l_1 + l_2} + m_{\mathrm{w}}\right)r_{33} - \frac{g\,(m_w R_w + 0.25\,m_{\mathrm{BC}}\,z_C)}{w}\,r_{32} + \frac{2\,g\,(m_w R_w + 0.25\,m_{\mathrm{BC}}\,z_C)}{l_1 + l_2}\,r_{31} \tag{68}$$

$$\zeta_{\mathrm{FL},11} = -\frac{1}{2}\left(\frac{{}^{\mathrm{B_C}}I_{\mathrm{yz}}}{l_1+l_2} - \frac{{}^{\mathrm{B_C}}I_{\mathrm{xz}}}{2\,w}\right)\ddot{\Psi} \tag{105}$$

$$\zeta_{\mathrm{FR},11} = -\frac{1}{2}\left(\frac{{}^{\mathrm{B_C}}I_{\mathrm{yz}}}{l_1+l_2} + \frac{{}^{\mathrm{B_C}}I_{\mathrm{xz}}}{2\,w}\right)\ddot{\Psi} \tag{106}$$

$$\zeta_{\mathrm{RR},11} = \frac{1}{2}\left(\frac{{}^{\mathrm{B_C}}I_{\mathrm{yz}}}{l_1+l_2} - \frac{{}^{\mathrm{B_C}}I_{\mathrm{xz}}}{2\,w}\right)\ddot{\Psi} \tag{107}$$

$$\zeta_{\mathrm{RL},11} = \frac{1}{2}\left(\frac{{}^{\mathrm{B_C}}I_{\mathrm{yz}}}{l_1+l_2} + \frac{{}^{\mathrm{B_C}}I_{\mathrm{xz}}}{2\,w}\right)\ddot{\Psi} \tag{108}$$

VIII. SIMULATION RESULTS

A. VALIDATING THE PROPOSED EXPRESSIONS

The presented derivation procedure and, consequently, the solutions for normal wheel loads have been based on the basic principles of rigid body dynamics with several reasonable assumptions introduced in the derivation process. As an external independent means for a self check-up, the Simscape Multibody$^{\mathrm{TM}}$ simulation will be used here to advocate the justifiability of the proposed modelling scheme and provide insights into how the introduced assumptions affect the final solution when they are not entirely valid. A 4AWD mobile manipulator in the simulation environment can be freely chosen because the equations are not tailored to any specific chassis shape or manipulator arm and their properties.

Notably, there exists a temporary inability to provide referent normal force values on an uneven, complex geometry terrain in the software used. State-of-the-art methods used to simulate a motion over an uneven terrain use clouds of points. Each contact force is based on the penetration and velocity of the individual point of the cloud. The Spatial Contact Force block does not support sensing when connected to a point cloud block, [47]. This fact has forced simulations here to be performed on a flat surface for the sake of providing an unbiased self-check comparison. Even these will suffice to highlight the benefits of monitoring wheel loads instead of tipping-over moments about pre-defined axes. In the case of uneven terrain, the argumentation brought out during the derivation process provides a firm basis regarding the temporary absence of unbiased self-check means. When the motion of a mobile manipulator is simulated over a flat surface, a spring-damper model for the soil can be used while ignoring the terrain geometry, as suggested and implemented in [48].

Thus, the reference values for the result comparisons and proof-of-concept purposes can be obtained relatively easy.

Flat-surface simulations are, in any case, significant when testing both static and dynamic terms at the same time. It is also expected that in the case of large angular velocities, more significant discrepancies between the referent results and the analytic ones will occur due to the introduced assumptions that neglect the wheel dynamics. These cases can be realistically simulated only on flat terrain. On uneven terrain, static terms will usually prevail because the manipulator will not have high linear/angular velocities in those cases.

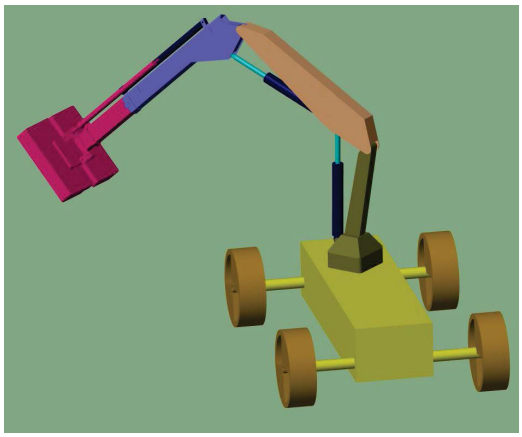

FIGURE 7. Simplified mobile manipulator in the Simscape Multibody$^{\mathrm{TM}}$ simulation environment used to justify the proposed modelling concept.

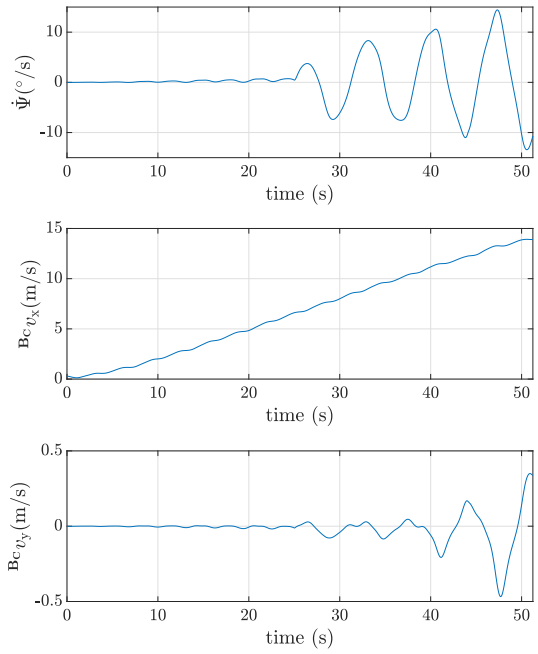

FIGURE 8. Linear/angular chassis velocities in the simulation.

The heavy-duty mobile manipulator shown in Fig. 7 will be used in the simulation. The manipulator arm will intentionally perform motions with significant angular accelerations to create ${}^{\mathrm{B_M}}\boldsymbol{F}$ components of a considerable magnitude. The simulation may exaggerate a situation that is likely to occur in practice but simultaneously tests the static and dynamic factors for a wider spectre of affecting values. All mass-related and other relevant physical properties of the manipulator arm can be found in [49], together with the detailed description of the calculation procedures for the forces. The other relevant simulation parameters are listed in Table 1.

The manipulator arm has also been intentionally oriented towards the front left wheel such that the rear right wheel is in the greatest danger of losing ground contact. This occurrence is one of those that are not likely to be detected using the

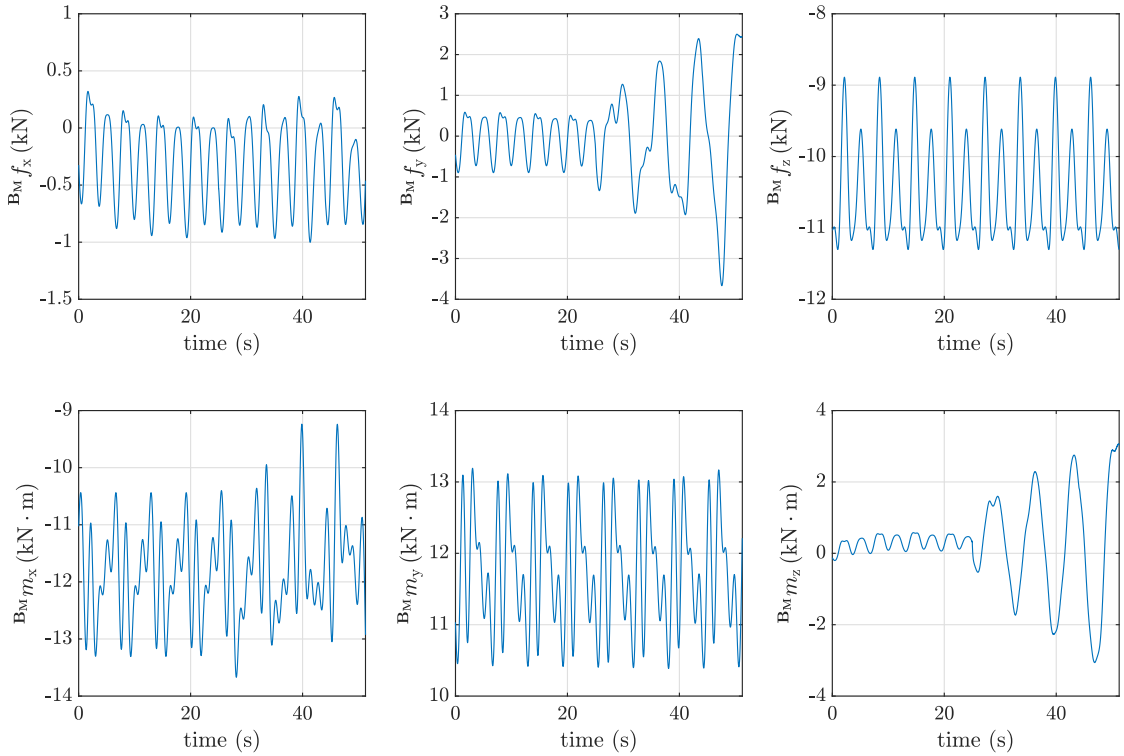

FIGURE 9. Forces and moments at the chassis/manipulator arm connection point, expressed as would have been measured in $\{\mathbf{B_M}\}$ frame.

TABLE 1. Wheeled platform parameters.

Label	Quantity	Value	Unit
m_{BC}	chassis mass	2200	kg
l_1	longitudinal distance between the chassis COM and rear axle	1.15	m
l_2	longitudinal distance between the chassis COM and front axle	1.15	m
w	lateral distance between the chassis COM and all the wheels	0.875	m
m_{w}	mass of the each wheel	60	kg
I_{zz}	chassis moment of inertia about the z-axis	1224	kg·m^2
R_{w}	radius of the each wheel	0.35	m
z_{C}	chassis COM height above the ground	0.45	m
x_{CA}	x-axis distance from (60)	0.5	m
y_{CA}	y-axis distance from (60)	0	m
z_{CA}	z-axis distance from (60)	0.25	m
g	gravity acceleration	9.8066	m/s^2

existing indicators, and thus, it is of primary interest here to reveal how the proposed approach prevails the ITOM and its predecessors.

Linear/angular chassis velocities in the simulated case are shown in Fig. 8. Forces/moments generated at the manipulator arm/chassis connection ${}^{\mathbf{B_M}}\boldsymbol{F}$ are shown in Fig. 9. Initially, these forces and moments are mainly caused by the motion of the manipulator arm and have been magnified by abrupt steering actions that are purposedly introduced to test the contribution of the angular velocity.

Values of the supporting forces calculated using the proposed approach, using (61) – (64) are shown in Fig. 10, along with the corresponding errors, and these results are significant from two viewpoints.

First, they show an excellent agreement between the simulation and analytic results. This fact proves the efficacy of the proposed extendable model with valid underlying assumptions. The proposed equations qualify as a good starting point for calculating the supporting forces considering the obtained matching with the Simscape Multibody$^{\mathrm{TM}}$ results. Although the discrepancies between the analytic and simulation results depend on more than introduced assumptions, such as on the solver choice, integration time, and soil model, for the investigated manoeuvre, the maximum absolute error is negligible at first, with a maximum value of approximately $130N$ as the motion becomes sharp, which is arguably more than acceptable considering the magnitudes of forces. The end-user can investigate the dissimilarities from the referent results and decide if a more complex model is required. In the absence of referent simulation or experimental results, the given methodology can be adopted in all the practical situations involving the considered class of mobile manipulators.

B. STABILITY CRITERIA IMPROVEMENTS

From the second standpoint, improvement with respect to the ITOM is noticeable. Namely, by observing the values for ${}^{\mathbf{T_{RR}}}f_z$, we can see that the rear right wheel loses contact with the surface at the point in time when the simulation

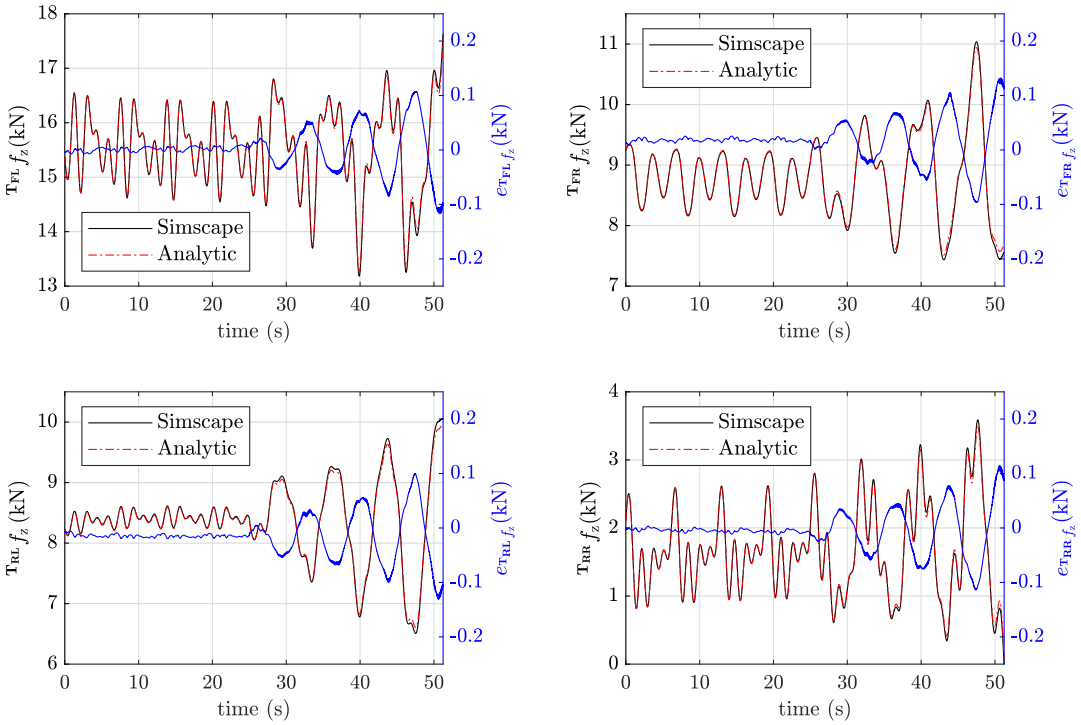

FIGURE 10. Wheel supporting forces on all wheels. The analytical results are compared with referent values from the Simscape Multibody™, and the corresponding error plots are given. The tip-over danger can be detected most appropriately by monitoring the supporting forces separately.

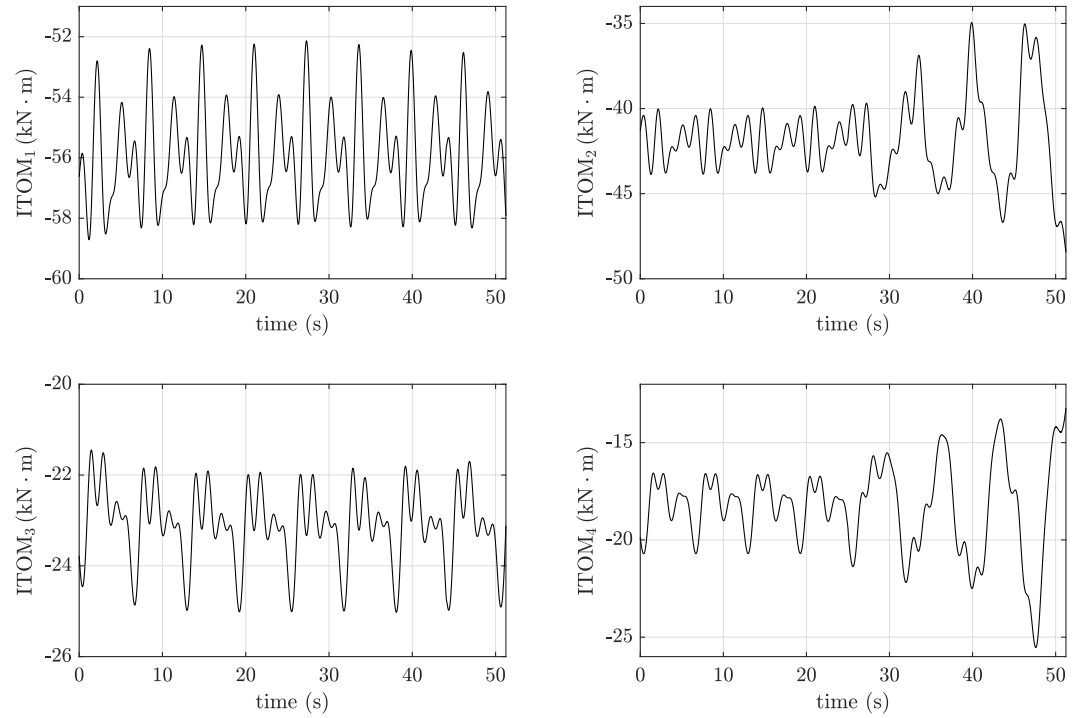

FIGURE 11. Values of the ITOM tip-over stability indicator. Negative ITOM values designate the tip-over stability. By considering only tipping-over about the axes connecting wheels, it cannot detect the case in which only one wheel loses contact with the ground.

ends. The convention in the ITOM tip-over stability indicator is such that the negative values imply the tip-over stability. The transition from the negative to positive ITOM values can occur only when the two wheels lose contact with the ground.

As shown in Fig. 11, although a positive gradient in some may exist, the highest ITOM indicator value is far below zero, indicating strong tip-over stability when the rear right wheel loses contact with the ground.

Monitoring the supporting forces per the suggested equations is intuitive and proved to be a better choice than monitoring the tipping-over moments about particular axes, no matter how detailed the underlying dynamics model is. The overturning force (OTF) stability measure emerges smoothly from the ongoing discussion as a simple alternative to ITOM. In contrast to the established procedures of comparing tipping-over moments, a comparison of the overturning forces with the prescribed stability margins is proposed. The overturning force is simply a wheel supporting force, which is given as follows:

$$\mathrm{OTF}_i = {}^{\mathbf{Ti}}f_z, \tag{109}$$

where $i = \mathrm{FL}, \mathrm{FR}, \mathrm{RR}, \mathrm{RL}$. For a reasonably chosen optimal margins $\mathrm{OTF}_{i,\mathrm{opt}}$, one can now similarly write:

$$\mathrm{OTF}_i = \mathrm{OTF}_{i,\mathrm{opt}} + \Delta\mathrm{OTF}_i. \tag{110}$$

The tip-over avoidance function from [22] can be easily swapped with the following:

$$\sigma = \frac{1}{2}\sum_i ||\Delta\mathrm{OTF}_i||_2^2, \tag{111}$$

$i = \mathrm{FL}, \mathrm{FR}, \mathrm{RR}, \mathrm{RL}$. This introduces the benefit of having analytically partial derivatives $\dfrac{\partial\sigma}{\partial\xi}$ which are used in the tip-over avoidance scheme which has already been proven to work, with $\xi = \left({}^{\mathbf{Bc}}v_{\mathrm{x}}\ {}^{\mathbf{Bc}}v_{\mathrm{y}}\ \dot{\Psi}\right)^T$. In light of the performed analysis, it is also more relevant to choose a $\mathrm{OTF}_{i,\max}$ margin.

C. PARAMETRIC UNCERTAINTY ANALYSIS

Because the presented study dominantly focusses on mathematical modelling and formulation of the wheel supporting forces, the implication of change in various parameters must be considered. An analysis like this can also be helpful to simultaneously test the exactness of the proposed expressions in a separate uncorrelated manoeuvre. In the parametric uncertainty analysis, the mobile manipulator will move forward until it stops and will then resume its motion in reverse when the steering action is also applied. The manipulator arm's orientation is kept the same as in the previous example. The manipulator velocities during this manoeuvre are shown in Fig. 12. All the relevant parameters are randomly varied in the range $\pm 10\%$ of their nominal values; these parameters are the lengths, angles, masses, and moments of inertia. Again, joint motions in the manipulator arm have been commanded using a set of uncorrelated sinusoidal changes with significant gradients.

Fig. 13 shows the shaded area between the largest and smallest error for forces/moments ${}^{\mathbf{BM}}f_x$, ${}^{\mathbf{BM}}f_y$, ${}^{\mathbf{BM}}f_z$, ${}^{\mathbf{BM}}m_x$, ${}^{\mathbf{BM}}m_y$, ${}^{\mathbf{BM}}m_z$ at the manipulator arm base and Fig. 14 does the same for all the wheel supporting forces ${}^{\mathbf{TFL}}f_z$, ${}^{\mathbf{TFR}}f_z$, ${}^{\mathbf{TRR}}f_z$, ${}^{\mathbf{TRL}}f_z$.

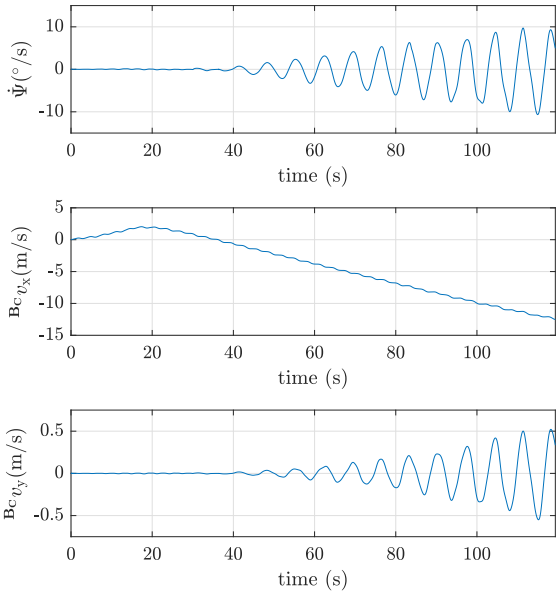

FIGURE 12. Linear/angular manipulator velocities during the simulations in which the effect of parameter uncertainties has been investigated.

Each force/moment error is defined as the difference between the force/moment value obtained using unexact relevant parameters, and the exact value provided by Simscape™. Fig. 13 indicates that, as expected, when discussing the manipulator arm base forces, parametric uncertainties mainly affect the force normal to the chassis and overturning moments. The reasons are comprehensible since the manipulator arm weighs approximately 1000 kg, and a 10% error in the manipulator arm mass introduces an error of approximately 1 kN that can only be increased in the considered test conditions with significant accelerations of arm links. The manipulator arm creates overturning moments, which can be erroneously calculated if the manipulator masses are not known precisely along with moment arms. Illustrating this in numbers, a 50 kg error in mass at the moment arm of 2 m introduces an error of approximately 1 kNm. Again, because all the possible manipulator parameters were varied and accelerations were significant, the error had understandable magnitudes. It is also noticeable that the moment error about the axis parallel to the chassis rotation axis eventually increases when the chassis angular velocity grows. Examining each of the 11 relevant terms one by one makes it clear how these errors are distributed to the supporting force errors. Further, the eventual 10% chassis mass error in the considered example indicates that an error of 2 kN is introduced and is distributed partially to each wheel. Thus, the magnitudes of the errors shown in Fig. 14 can be justified.

What makes the presented parametric uncertainty analysis interesting is to show that, as expected, the magnitudes of the errors for the FL and RR wheels are large. Differences in the error ranges are expected considering that the orientation of the manipulator arm is again as shown in Fig. 7. It is

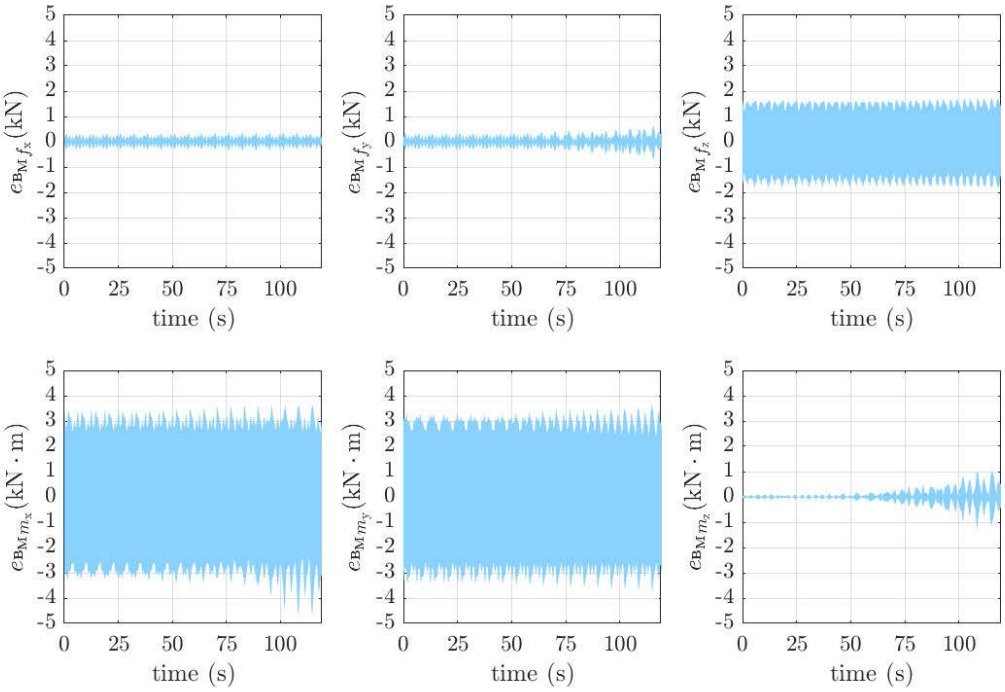

FIGURE 13. Error ranges in the manipulator arm base force/moments when the relevant geometric and mass properties are known up to ±10% of nominal values.

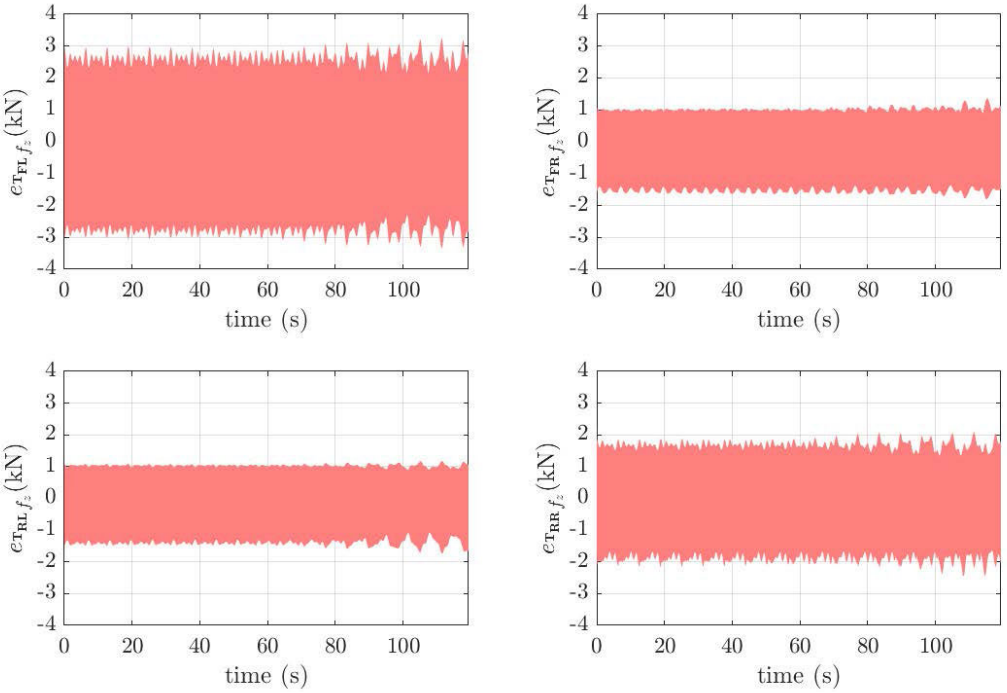

FIGURE 14. Error ranges in the supporting wheel forces when the relevant geometric and mass properties are known up to ±10% of nominal values.

valid to conclude that when accounting for some error safety margin, limiting cases with largest errors should be found from the predicted workspace. This error margin should be included as fixed or adaptively in the overturning stability criterion. It could make the criterion more conservative, but we must try to avoid cases in which the prescribed force limit is undetectably reached in the presence of parametric uncertainties.

In the sketchy mobile manipulator considered in the present study, the chassis mass and its COM position, along with the manipulator arm position and orientation, are chosen such that the extreme case of losing the terrain contact can be investigated relatively easily. Such a simulation setting and tracing zero supporting forces are very convenient for proof-of-concept purposes when discussing the magnitudes of normal forces and the benefits of monitoring these in contrast to overturning moments.

The sensitivity of the overturn danger anticipation and overturn preventing algorithms to parametric uncertainty on an uneven terrain would require a completely separate analysis considering the required amount of work. It would also be convenient to conduct it with a realistic wheeled platform design where the supporting forces are better balanced between wheels in the nominal working posture. In addition, sensor nonidealities, sensor data fusion and other related topics, together with their effect, should be investigated.

All the simulations were run on a machine with Intel® Core™ i5-10310U CPU @1.70 GHz and 16.0 GB RAM in MATLAB® 2021b for academic use.

IX. DISCUSSION

When simulating the motion of different mobile manipulator configurations over flat or uneven terrain, some spring-damper soil models are known to provide reliable results for normal forces. These contact models are widely accepted in the robotics community. A wide range of studies for various steering configurations is available with remarkable dynamics models but with expressions for normal forces relying on the tyre-soil contact dynamics. If these values for normal wheel forces are to be used inside the simulation environment, most often, for modelling the other tyre force/moments, no objection can be made about them. In practice, multiple benefits could be obtained if the supporting forces were monitored during the operation. One significant improvement addressed here in detail could be the better assessment of the overturning stability. The performance of the mobile manipulator could additionally benefit from performing additional on-line calculations where the wheel supporting forces participate. Direct measurement of the supporting forces usually falls out of the scope because the force sensors are expensive and unresistant to shocks, which must be especially considered with heavy-duty working machines. In these cases, the tyre-soil contact models may also be an unreliable and impractical choice. The first reason is that the tyre/spring deformations may be difficult/expensive to measure considering the nature of the quantities and the range of the expected measured values. The other reason is that the tyre/spring stiffnesses must be known perfectly, and the solution becomes very sensitive to changes in this parameter since all the results largely depend on it. Expressing the normal wheel forces in terms of quantities that are likely to be measured with much higher accuracy during the mobile manipulator operation, like linear/angular velocities and accelerations, is much more reasonable. Combining on-line measurable quantities with other physical quantities, whose values are likely to be known in advance with a relatively high degree of accuracy, is the primary goal that the research community must set and prioritize. The present study gives a solution like this for a class of 4-wheeled mobile manipulators with rigid chassis. Ready-to-use analytic results like this for supporting wheel forces in 4-wheeled mobile manipulators with rigid chassis cannot be found in the existing literature on mobile manipulator dynamics. Although the opposite case may be argued, obtaining these expressions does not pose a significant challenge if the line of thought commonly employed in vehicle dynamics is followed. After the careful formulation of subsystem-by-subsystem dynamics, using the compact 6D vector form, which explicitly includes the ground reaction forces, an appropriate system of equations with tyre loads as unknowns can be formed. The EOMs in which normal loads participate are initially hard to handle and provide highly impractical solutions. An elegant, easy-to-solve system is obtained by carefully combining these with the remaining EOMs. With reasonable assumptions, the solution for each normal force is a neat sum of 11 terms that accurately captures the normal load changes. This sum can be potentially simplified further or made even more complex from case to case if required. It is highly likely that the wheel dynamics will be neglected and that, consequently, the given compact sums that approximate the exact solutions can be readily used because these do not depend on the steering principles. Even if it is determined that wheel dynamics must be included in the calculation of normal forces, the proposed approach leads to the most general solution possible, which is significantly more complex.

An independent comparison of the obtained analytical results with the results obtained using Simscape Multibody™ for one random wheeled platform with a heavy-duty serial-parallel manipulator on top verifies the adequacy of the proposed equations. It must be emphasised that the normal forces in the simulation have been modelled using the spring-damper model. Result comparison proves that the same results can be obtained using these two different approaches where the one using equations derived here is more likely to be the one chosen for practical applications.

As the extremely important field of application for these expressions, the community must consider overturning stability and prevention analyses.

In contrast to the existing tipping-over stability criteria, from now on, normal loads can be relatively easily imported to tip-over stability analysis. This new opportunity of inclusion offers significant effectivity. The assumptions on the tipping-over axis can be removed finally. A simple consequence is that all the possible underlying causes of overturning (in)stability are comprehended when working in terms of forces. Furthermore, it is intuitively clear that prescribing relative stability margins in terms of forces is more accessible and straightforward than overturning moments about different axes, which brings the derived results close to the broader audience of readers and end-users.

X. CONCLUSION

Expressions for normal wheel loads based on the tyre-soil contact dynamics are a proven modelling choice for simulation purposes of wheeled platforms such as cars and mobile manipulators. For on-line monitoring of tyre supporting forces, these are likely to be hardly applicable or inapplicable. This fact did not raise much concern in the community of mobile manipulators, especially when considering 4- or more-wheeled configurations. Instead of monitoring normal wheel forces when assessing the manipulator overturning stability, overturning moments about the fixed axes were more commonly considered, and stability criteria were built upon these. Such an approach relies on the action and reaction principle where moments made by the wheel supporting forces about axes connecting wheels can be calculated, but particular values for each of them are not obtainable. The present study showed, using an example of a 4-wheeled rigid-chassis mobile manipulator, how monitoring the normal forces provides significant benefits and in certain situations anticipates the overturning danger much better than the methods based on the overturning moments. In light of this, it is clear that reformulations of expressions for normal wheel loads in terms of linear/angular velocities along with reliable geometric and mass quantities are highly desirable.

We show how specific car dynamics modelling approaches can be systematically extended to one class of mobile manipulators. It can also be expected that many more will follow for different configurations not addressed here, following the same line of thought.

With the closed gap between the car dynamics and mobile manipulators for the analytical determination of the wheel supporting forces, new tipping-over criteria and tipping-over avoidance schemes can be formed.

Modifiable analytic expressions like the ones presented here seem to be a logical continuation of ongoing efforts in the research community and should represent the first step in modifying the overturning stability criteria, naturally, in terms of normal wheel loads.

The present study also calls for the detailed analysis of uneven terrain because it is known to introduce certain modelling errors and has not received enough attention over the years. With the discussion of an uneven terrain effect in more detail, we suggest investigating tipping-over stability indicators, which also emphasise the terrain configuration since these may present an exciting and significant improvement to the existing ones.

ACKNOWLEDGMENT

The authors express their gratitude to Dr. Janne Koivumäki and Lionel Hulttinen for providing positive criticism and constructive feedback for improving the content of the article and the material presentation. The content of this article does not reflect the official opinion of the Shift2Rail Joint Undertaking (S2R JU). The content of this work reflects only the author's view, and the JU is not responsible for any use that may be made of the information it contains.

REFERENCES

[1] Y. Liu and G. Liu, "Interaction analysis and online tip-over avoidance for a reconfigurable tracked mobile modular manipulator negotiating slopes," *IEEE/ASME Trans. Mechatronics*, vol. 15, no. 4, pp. 623–635, Aug. 2010, doi: 10.1109/TMECH.2009.2031174.

[2] J. Mattila, J. Koivumaki, D. G. Caldwell, and C. Semini, "A survey on control of hydraulic robotic manipulators with projection to future trends," *IEEE/ASME Trans. Mechatronics*, vol. 22, no. 2, pp. 669–680, Apr. 2017, doi: 10.1109/TMECH.2017.2668604.

[3] S. Aguilera-Marinovic, M. Torres-Torriti, and F. Auat-Cheein, "General dynamic model for skid-steer mobile manipulators with wheel–ground interactions," *IEEE/ASME Trans. Mechatronics*, vol. 22, no. 1, pp. 433–444, Feb. 2017, doi: 10.1109/TMECH.2016.2601308.

[4] K. Shigematsu, T. Tsubouchi, and S. Sarata, "Tip-over prevention system based on motion prediction for teleoperated excavator," *Adv. Robot.*, vol. 35, no. 23, pp. 1438–1449, Nov. 2021, doi: 10.1080/01691864.2021.2004223.

[5] A. T. Fuentes, M. Kipfmüller, C. Burghart, M. A. José Prieto, T. Bertram, M. Bryg, and T. Bergmann, "Stable operation of arm type robots on mobile platforms," *Proc. CIRP*, vol. 99, pp. 104–109, Jan. 2021, doi: 10.1016/j.procir.2021.03.017.

[6] T. Song, F. Xi, S. Guo, and Y. Lin, "Optimization of a mobile platform for a wheeled manipulator," *J. Mech. Robot.*, vol. 8, no. 6, pp. 1–14, Dec. 2016, doi: 10.1115/1.4033855.

[7] M. Vukobratović and B. Borovac, "Zero-moment point—Thirty five years of its life," *Int. J. Hum. Robot.*, vol. 1, no. 1, pp. 157–173, Mar. 2004, doi: 10.1142/S0219843604000083.

[8] S. Sugano, Q. Huang, and I. Kato, "Stability criteria in controlling mobile robotic systems," in *Proc. IEEE/RSJ Int. Conf. Intell. Robots Syst. (IROS)*, Yokohama, Japan, Jul. 1993, pp. 832–838, doi: 10.1109/IROS.1993.583186.

[9] J. Kim, W. K. Chung, Y. Youm, and B. H. Lee, "Real-time ZMP compensation method using null motion for mobile manipulators," in *Proc. IEEE Int. Conf. Robot. Automat. (ICRA)*, Washington, DC, USA, May 2002, pp. 1967–1972, doi: 10.1109/ROBOT.2002.1014829.

[10] P. R. Roan, A. Burmeister, A. Rahimi, K. Holz, and D. Hooper, "Real-world validation of three tipover algorithms for mobile robots," in *Proc. IEEE Int. Conf. Robot. Autom.*, Anchorage, AK, USA, May 2010, pp. 4431–4436, doi: 10.1109/ROBOT.2010.5509506.

[11] M. H. Korayem, V. Azimirad, A. Nikoobin, and Z. Boroujeni, "Maximum load-carrying capacity of autonomous mobile manipulator in an environment with obstacle considering tip over stability," *Int. J. Adv. Manuf. Technol.*, vol. 46, no. 5, pp. 811–829, Jan. 2010, doi: 10.1007/s00170-009-2146-0.

[12] J. Song and I. Sharf, "Time optimal motion planning with ZMP stability constraint for timber manipulation," in *Proc. IEEE Int. Conf. Robot. Automat. (ICRA)*, Paris, France, May 2020, pp. 4934–4940, doi: 10.1109/ICRA40945.2020.9196836.

[13] A. Argiolas, S. Casini, K. Fujio, T. Hiramatsu, S. Morita, M. Ragaglia, H. Sugiura, and M. Niccolini, "Design, development and validation of a dynamic fall prediction system for excavators," in *Proc. IEEE Int. Conf. Robot. Autom. (ICRA)*, Xi'an, China, May 2021, pp. 8523–8529, doi: 10.1109/ICRA48506.2021.9560796.

[14] Y. de Viragh, M. Bjelonic, C. D. Bellicoso, F. Jenelten, and M. Hutter, "Trajectory optimization for wheeled-legged quadrupedal robots using linearized ZMP constraints," *IEEE Robot. Autom. Lett.*, vol. 4, no. 2, pp. 1633–1640, Apr. 2019, doi: 10.1109/LRA.2019.2896721.

[15] E. G. Papadopoulos and D. A. Rey, "A new measure of tipover stability margin for mobile manipulators," in *Proc. IEEE Int. Conf. Robot. Autom.*, Minneapolis, MN, USA, Apr. 1996, pp. 3111–3116, doi: 10.1109/ROBOT.1996.509185.

[16] D. A. Rey and E. G. Papadoupoulos, "Online automatic tipover prevention for mobile manipulators," in *Proc. IEEE/RSJ Int. Conf. Intell. Robot Systems. Innov. Robot. Real-World Appl. (IROS*, Grenoble, France, Sep. 1997, pp. 1273–1278, doi: 10.1109/IROS.1997.656414.

[17] S. A. A. Moosavian and K. Alipour, "On the dynamic tip-over stability of wheeled mobile manipulators," *Int. J. Robot. Autom.*, vol. 22, no. 4, pp. 322–328, 2007, doi: 10.2316/Journal.206.2007.4.206-3036.

[18] K. Alipour, A. Hasanpour, and P. Daemy, "Comparing two online tip-over avoidance algorithms for mobile manipulators," in *Proc. 2nd RSI/ISM Int. Conf. Robot. Mechatronics (ICRoM)*, Tehran, Iran, Oct. 2014, pp. 310–315, doi: 10.1109/ICRoM.2014.6990919.

[19] S. Guo, T. Song, F. Xi, and R. P. Mohamed, "Tip-over stability analysis for a wheeled mobile manipulator," *J. Dyn. Syst., Meas., Control*, vol. 139, no. 5, pp. 1–7, May 2017, doi: 10.1115/1.4035234.

[20] X. Li, L. Wu, Q. Sun, and T. Song, "Online dynamic tip-over analysis for a wheeled mobile dual-arm robot with an improved tip-over moment stability criterion," *J. Robot.*, vol. 2021, pp. 1–11, Jul. 2021, doi: 10.1155/2021/9913335.

[21] C. J. Lee, J. Lee, and S. Rhim, "Design of maximum stopping deceleration of mobile manipulator considering the protective separation distance without tip-over," in *Proc. IEEE Int. Conf. Intell. Safe. Robot. (ISR)*, Tokoname, Japan, Mar. 2021, pp. 326–329, doi: 10.1109/ISR50024.2021.9419546.

[22] X. Ding, Y. Liu, J. Hou, and Q. Ma, "Online dynamic tip-over avoidance for a wheeled mobile manipulator with an improved tip-over moment stability criterion," *IEEE Access*, vol. 7, pp. 67632–67645, 2019, doi: 10.1109/ACCESS.2019.2915115.

[23] R. Jazar, "Weight transfer," in *Advanced Vehicle Dynamics*, 1st ed. Cham, Switzerland: Springer, 2019, pp. 88–104, ch. 1, sec. 7, doi: 10.1007/978-3-030-13062-6.

[24] H. B. Pacejka and I. J. M. Besselink, "Magic formula tyre model with transient properties," *Vehicle Syst. Dyn.*, vol. 27, no. 1, pp. 234–249, 1997, doi: 10.1080/00423119708969658.

[25] I. J. M. Besselink, A. J. C. Schmeitz, and H. B. Pacejka, "An improved magic formula/swift tyre model that can handle inflation pressure changes," *Vehicle Syst. Dyn.*, vol. 48, pp. 337–352, Dec. 2010, doi: 10.1080/00423111003748088.

[26] Y. Li, "Dynamic stability analysis and control for the mobile manipulator," in *Proc. IEEE CCECE. Can. Conf. Electr. Comput. Eng. Conf.*, Winnipeg, MB, Canada, May 2002, pp. 554–559, doi: 10.1109/CCECE.2002.1015287.

[27] J. A. Souza-Jimenez, E. Zavala-Pacheco, J. C. Garcia-Hernandez, and V. J. Gonzalez-Villela, "Tip-over stability estimation of a mobile manipulator using the mean normal ground reaction criterion," in *Proc. Int. Conf. Mechatron. Electro. Auto. Eng. (ICMEAE)*, Cuernavaca, Mexico, Nov. 2020, pp. 137–141, doi: 10.1109/ICMEAE51770.2020.00031.

[28] Y. Liu and Y. Liu, "Real-time tip-over prevention and path following control for redundant nonholonomic mobile modular manipulators via fuzzy and neural-fuzzy approaches," *J. Dyn. Syst., Meas., Control*, vol. 128, no. 4, pp. 753–764, Dec. 2006, doi: 10.1115/1.2229253.

[29] Y. Li and Y. Li, "Kinematics and tip-over stability analysis for the mobile modular manipulator," *Proc. Inst. Mech. Eng., C, J. Mech. Eng. Sci.*, vol. 219, no. 3, pp. 331–342, Mar. 2005, doi: 10.1243/095440605X16866.

[30] X. Chen, W. Chen, L. Hou, H. Hu, X. Bu, and Q. Zhu, "A novel data-driven rollover risk assessment for articulated steering vehicles using RNN," *J. Mech. Sci. Technol.*, vol. 34, no. 5, pp. 2161–2170, Apr. 2020, doi: 10.1007/s12206-020-0437-4.

[31] X. Li, Y. Wu, W. Zhou, and Z. Yao, "Study on roll instability mechanism and stability index of articulated steering vehicles," *Math. Problems Eng.*, vol. 2016, pp. 1–15, Apr. 2016, doi: 10.1155/2016/7816503.

[32] Z. Sun, D. Zhang, Z. Li, Y. Shi, and N. Wang, "Optimum design and trafficability analysis for an articulated wheel-legged forestry chassis," *J. Mech. Design*, vol. 144, no. 1, Jan. 2022, Art. no. 013301, doi: 10.1115/1.4051539.

[33] G. Gilardi and I. Sharf, "Literature survey of contact dynamics modelling," *Mech. Mach. Theory*, vol. 37, no. 10, pp. 1213–1239, Oct. 2002, doi: 10.1016/S0094-114X(02)00045-9.

[34] R. Jazar, "Motion dynamics," in *Theory of Applied Robotics: Kinematics, Dynamics, and Control*, 2nd ed. New York, NY, USA: Springer, 2010, pp. 581–628, ch. 11, sec. 1–8, doi: 10.1007/978-1-4419-1750-8.

[35] R. Featherstone, "A beginner's guide to 6-D vectors (Part 1)," *IEEE Robot. Autom. Mag.*, vol. 17, no. 3, pp. 83–94, Sep. 2010, doi: 10.1109/MRA.2010.937853.

[36] W. H. Zhu, *Virtual Decomposition Control: Toward Hyper Degrees Freedom Robots*, 1st ed., Berlin, Germany: Springer-Verlag, 2010, doi: 10.1007/978-3-642-10724-5.

[37] G. R. Petrović and J. Mattila, "Mathematical modelling and virtual decomposition control of heavy-duty parallel–serial hydraulic manipulators," *Mech. Mach. Theory*, vol. 170, Jan. 2022, Art. no. 104680, doi: 10.1016/j.mechmachtheory.2021.104680.

[38] W. H. Zhu, "Rigid body dynamics in a body frame," in *Virtual Decomposition Control: Toward Hyper Degrees Freedom Robots*, 1st ed. Berlin, Germany: Springer-Verlag, 2010, pp. 30–31, ch. 2, sec. 6, doi: 10.1007/978-3-642-10724-5.

[39] B. L. Stevens, F. L. Lewis, and E. N. Johnson, "Rigid body dynamics," in *Aircraft Control and Simulation: Dynamics, Controls Design, and Autonomous Systems*, 3rd ed. Hoboken, NJ, USA: Wiley, 2015, pp. 34–44, ch. 1, sec. 7, doi: 10.1002/9781119174882.

[40] V. Wiberg, E. Wallin, T. Nordfjell, and M. Servin, "Control of rough terrain vehicles using deep reinforcement learning," *IEEE Robot. Autom. Lett.*, vol. 7, no. 1, pp. 390–397, Jan. 2022, doi: 10.1109/LRA.2021.3126904.

[41] R. Jazar, "Vehicles on a crest and dip," in *Vehicle Dynamics: Theory and Application*, 1st ed. Boston, MA, USA: Springer, 2008, pp. 78–87, ch. 2, sec. 8, doi: 10.1007/978-0-387-74244-1.

[42] W. F. Milliken and D. L. Milliken, "Other terrain effects," in *Race Car Vehicle Dynamics*, 3rd ed. Warrendale, PA, USA: Society of Automotive Engineers, 1995, pp. 690–694, ch. 18, sec. 7.

[43] R. Jazar, "Four-wheel planar vehicle dynamics," in *Advanced Vehicle Dynamics*, 1st ed. Cham, Switzerland: Springer, 2019, p. 173, ch. 2, sec. 6, doi: 10.1007/978-3-030-13062-6.

[44] R. Jazar, "Wheel and tire coordinate frames," in *Advanced Vehicle Dynamics*, 1st ed. Cham, Switzerland: Springer, 2019, pp. 1–13, ch. 1, sec. 1, doi: 10.1007/978-3-030-13062-6.

[45] A. Obradovic, S. Salinic, and R. Radulovic, "The brachistochronic motion of a vertical disk rolling on a horizontal plane without slip," *Theor. Appl. Mech.*, vol. 44, no. 2, pp. 237–254, 2017, doi: 10.2298/TAM171002015O.

[46] G. Perantoni and D. J. N. Limebeer, "Optimal control for a formula one car with variable parameters," *Vehicle Syst. Dyn., Int. J. Vehicle Mech. Mobility*, vol. 52, no. 5, pp. 653–678, 2014, doi: 10.1080/00423114.2014.889315.

[47] (2022). *Point Cloud*. MathWorks. Accessed: Apr. 3, 2022. [Online]. Available: https://www.mathworks.com/help/physmod/sm/ref/pointcloud.html

[48] (2022). *Simscape Vehicle Templates*. Steve Miller. Accessed: Apr. 3, 2022. [Online]. Available: https://github.com/mathworks/Simscape-Vehicle-Templates/releases/tag/21.2.2.6

[49] (2022). *Hydraulic Manipulator Arm Forces Modelling*. Goran Petrović. Accessed: Apr. 3, 2022. [Online]. Available: https://github.com/petrovicrgoran/ForcesModelling

GORAN R. PETROVIĆ was born in Novi Pazar, SFR Yugoslavia, in 1990. He received the B.S. and M.S. degrees in control engineering from the Faculty of Mechanical Engineering, University of Belgrade, Republic of Serbia, in 2014. From March 2015 to March 2021, he was a Teaching Assistant at the Control Group, Faculty of Mechanical Engineering, University of Belgrade. Since April 2021, he has been a Postdoctoral Researcher with the Faculty of Engineering and Natural Sciences, Unit of Automation Technology and Mechanical Engineering, Tampere University, under the supervision of Prof. Jouni Mattila. His research interests include mobile manipulators, electro-hydraulic actuation, and nonlinear model-based control algorithms. He graduated as the best in his class and was a recipient of the Serbian Ministry of Youth and Sports Scholarship—Dositeja, awarded to the 1000 best students in the Republic of Serbia.

JOUNI MATTILA received the M.Sc. (Eng.) and Dr.Tech. degrees from the Tampere University of Technology (TT), Tampere, Finland, in 1995 and 2000, respectively. He is currently a Professor of machine automation with the Unit of Automation Technology and Mechanical Engineering, Tampere University. His research interests include machine automation, nonlinear model-based control of robotic manipulators, and energy-efficient control of heavy-duty mobile manipulators.